

Ω_0 and substructure in galaxy clusters

David A. Buote[★]

Institute of Astronomy, Madingley Road, Cambridge CB3 0HA

1 February 2008

ABSTRACT

We examine the theoretical relationship between Ω_0 and substructure in galaxy clusters which are formed by the collapse of high density peaks in a gaussian random field. The radial mass distributions of the clusters are computed from the spherical accretion model using the adiabatic approximation following Ryden & Gunn. For a cluster of mass, $M(r, t)$, we compute the quantity $\Delta M / \bar{M}$ at a cosmic time t and within a radius r , where ΔM is the accreted mass and \bar{M} is the average mass of the cluster during the previous relaxation time, which is computed individually for each cluster. For a real cluster in three dimensions we argue that $\Delta M / \bar{M}$ should be strongly correlated with the low order multipole ratios, $\Phi_l^{int} / \Phi_0^{int}$, of the potential due to matter interior to r . Because our analysis is restricted to considering only the low order moments in the gravitational potential, the uncertainty associated with the survival time of substructure is substantially reduced in relation to previous theoretical studies of the “frequency of substructure” in clusters.

We study the dependence of $\Delta M / \bar{M}$ on radius, mass, Ω_0 , $\lambda_0 = 1 - \Omega_0$, redshift, and relaxation timescale in universes with Cold Dark Matter (CDM) and power-law power spectra. The strongest dependence on Ω_0 ($\lambda_0 = 0$) occurs at $z = 0$ where $\Delta M / \bar{M} \propto \Omega_0^{1/2}$ for relaxation times $\sim 1 - 2$ crossing times and only very weakly depends on mass and radius. The fractional accreted mass in CDM models with $\Omega_0 + \lambda_0 = 1$ depends very weakly on Ω_0 and has a magnitude similar to the $\Omega_0 = 1$ value. $\Delta M / \bar{M}$ evolves more rapidly with redshift in low-density universes and decreases significantly with radius for $\Omega_0 = 1$ models for $z \gtrsim 0.5$. We discuss how to optimize constraints on Ω_0 and λ_0 using cluster morphologies.

It is shown that the expected correlation between $\Delta M / \bar{M}$ and $\Phi_l^{int} / \Phi_0^{int}$ extends to the two-dimensional multipole ratios, $\Psi_m^{int} / \Psi_0^{int}$, which are well defined observables of the cluster density distribution. We describe how N-body simulations can quantify this correlation and thus allow $\Delta M / \bar{M}$ to be measured directly from observations of cluster morphologies.

Key words: galaxies: clusters: general – galaxies: evolution – galaxies: structure – cosmology: theory – X-rays: galaxies.

1 INTRODUCTION

Clusters of galaxies have proven to be useful laboratories for cosmological studies and have in particular yielded interesting measurements of Ω_0 , the present value of the average mass (energy) density of the universe expressed in terms of the critical density required for closure. The methods to measure Ω_0 with clusters each have their own advantages and disadvantages (see Dekel, Burstein, & White 1997). Perhaps the most familiar method is to assume the mass-to-light ratio in clusters is representative of the universe as a whole

(Carlberg, Yee, & Ellingson 1997). This method is popular because of its conceptual simplicity and relative ease to implement, but the basic assumption of this method may be unjustified. Another promising method uses the abundances of clusters (e.g. White, Efstathiou, & Frenk 1993) to derive a relationship between Ω_0 and σ_8 , the rms fluctuations in mass within spheres of radius $8h^{-1}$ Mpc. This method has the advantage that the theoretical comparison can be usefully achieved by relatively simple and computationally inexpensive semi-analytical methods. One disadvantage of this method is that cluster masses are usually determined from X-ray temperatures, the relationship of which is not entirely certain. Another disadvantage is the uncertainty in σ_8 due

[★] E-mail: buote@ast.cam.ac.uk

the uncertainty in the bias factor for clusters (Mo, Jing, & White 1997).

The detailed structure of clusters provides a complementary constraint on Ω_0 . Although the radial density profiles of clusters appear to be very insensitive to Ω_0 when scaled in terms of their virial radii (Navarro, Frenk, & White 1997), the presence of substructure in the mass distribution appears to be a quite sensitive diagnostic of Ω_0 as suggested in the pioneering study by Richstone, Loeb, & Turner (1992). Advantages of this method include the direct influence of Ω_0 on cluster morphologies (i.e. growth of structure regulated by Ω_0), and cluster morphologies are straightforward to quantify and compute observationally (e.g. Buote & Tsai 1995). The principal disadvantage is that a proper theoretical model requires computationally expensive high-resolution N-body simulations of a *large* number of clusters sufficient to adequately sample the variety of spatial morphologies of a cluster population (Jing et al. 1995; Buote & Xu 1997; Thomas et al. 1997).

To date the only study that has compared the requisite large N-body simulations to observations is Buote & Xu (1997; hereafter BX). Using dissipationless simulations of scale-free and Cold Dark Matter (CDM) models (e.g. Ostriker 1993) and X-ray data of clusters from ROSAT, BX determined that the spatial morphologies of galaxy clusters (1) decouple the influence of Ω_0 and the power spectrum when quantified in terms of statistics based on ratios of multipoles of the projected gravitational potential (Buote & Tsai 1995), and (2) favor a low matter density ($\Omega_0 \lesssim 0.3$). However, a rigorous determination of Ω_0 from X-ray cluster morphologies requires dissipational simulations of a statistically large number of clusters, at present a daunting computational expenditure even for only one set of model parameters[†]. To facilitate this process, less computationally intensive semi-analytic methods could be used to rapidly identify the optimum parameters (e.g. redshift, mass range, radius) of a cluster sample which maximize the ability to determine Ω_0 and possibly a cosmological constant via cluster morphologies.

A re-examination of semi-analytical[‡] models of the relationship between cluster morphologies and Ω_0 is important in its own right. As it is to be expected given the nature of the problem, semi-analytic approaches to cluster morphologies have been highly idealized. The previous studies do not actually construct model cluster mass distributions having substructure, but either adopt a spherical collapse model for computing a distribution of cluster collapse times (Richstone et al. 1992) or use simplified models of the merging histories of clusters to compute the distributions of times since a substantial merger event (Kauffmann & White 1993; Lacey & Cole 1993). Even if we accept such simplifications as necessary evils to be traded for intuitive guidance and increased computational speed, these models are of limited usefulness because they only compute the ambiguous “frequency of substructure” in clusters which is very sensitive

to the uncertain survival time of substructure (Kauffmann & White 1993; Lacey & Cole 1993).

In this paper we present an intuitive model for substructure, based on the spherical accretion model, that is closely related to quantitative observables of cluster morphology. We describe how N-body simulations can quantify the relationship between our model and the observables and thus allow a direct measurement of Ω_0 . However, for our present study, we use this model to (1) provide physical insight into the evolution of cluster morphology with redshift as a function of Ω_0 and $\lambda_0 = 1 - \Omega_0$ and to (2) assist the designing of future observing programs for the detailed comparison of these observational samples to clusters produced in N-body simulations. We then outline a procedure to optimize determination of Ω_0 and λ_0 using the observables of cluster morphology that are closely related to our model.

The paper is organized as follows. In §2 we motivate our model and show its relationship to quantitative observables of cluster morphology. The details of the spherical accretion model and the cosmological framework are discussed in §3 and §4 respectively. In §5 we analyze the model for different values of Ω_0 , λ_0 , and z for CDM and power-law power spectra. Finally, we discuss these results and identify the best ways to constrain Ω_0 and λ_0 observationally in §6.

2 MOTIVATION

2.1 Theory

In a standard Friedmann-Robertson-Walker universe with $\Omega_0 < 1$ and $\lambda_0 = 0$, the linear growth of density fluctuations becomes strongly suppressed when the curvature term in the Friedmann equation exceeds the matter term. The redshift delineating this transition from an Einstein - de Sitter phase to one of free expansion is then $1 + z_{trans} = \Omega_0^{-1} - 1$; i.e. when the matter density $\Omega(z_{trans}) = 0.5$. (e.g. §11B in Peebles 1980). Hence, if $\Omega_0 \ll 1$, then objects formed a long time in the past relative to universes where $\Omega_0 \approx 1$, and thus clusters in low-density universes should be, on average, more relaxed than clusters in universes with $\Omega_0 \approx 1$. To apply this idea to real clusters it is necessary to specify what it means for clusters to be “more relaxed”.

The most general stable self-gravitating non-rotating equilibrium configuration is the triaxial ellipsoid. Features like substructure that break this symmetry provide a measure of the departure of a cluster from a virialized state. The relaxation rate determines how rapidly substructure and other non-ellipsoidal features are erased in order to bring the system to equilibrium. Hence, the amount of substructure in a cluster at a particular epoch, or rather the degree of non-ellipsoidal symmetry, is approximately determined by the amount of mass accreted over the timescale associated with the relaxation rate.

This relaxation timescale depends on the mass distributions of the cluster and the subclumps (e.g. White & Rees 1978; Binney & Tremaine 1987), and is typically of order the crossing time of the system for substructures and non-ellipsoidal distortions comprising a substantial fraction ($\gtrsim 20\%$) of the cluster mass[§]. Since our interest lies in how

[†] Dissipationless simulations should be adequate for mass maps of clusters derived from gravitational lensing when such maps for observed clusters become widely available.

[‡] For our discussion we broadly define semi-analytical to be techniques other than three-dimensional N-body simulations.

[§] Mergers of structures of these sizes with clusters are typical for

much a cluster departs from a virialized state, we must consider how much a cluster evolves morphologically over the relaxation timescale, not just the amount of substructure present at a particular time.

If gravity drives the dynamical evolution of clusters, then we would expect the morphological evolution to be similar for clusters of different masses (approximately self-similar); i.e. the degree of morphological evolution should be proportional to the amount of accreted mass and inversely proportional to the total cluster mass. We write this fractional amount of mass accreted over a crossing time as $\Delta M / \bar{M}$, where ΔM is the accreted mass and \bar{M} is the average mass of the cluster within a radius r . We may write an equivalent expression in terms of the multipole moments of the gravitational potential due to matter interior to a radius r ,

$$\frac{\Delta M}{\bar{M}} = \frac{\Delta \Phi_0^{int}}{\bar{\Phi}_0^{int}}, \quad (1)$$

where $\Phi_0^{int} = -GM(< r)/r$ is the monopole term. Of course, substructure and other non-ellipsoidal distortions have important contributions to other moments of the potential, and we expect that the increase in the monopole will be strongly correlated with increases in the next few multipoles. (Indeed, this is the basis of our hypothesis that substructure is related to the amount of accreted mass over the relaxation timescale.) Hence, let us consider the increase in Φ^{int} , expanded in terms of all of its multipoles (and suppressing the azimuthal terms),

$$\frac{\Delta \Phi^{int}}{\bar{\Phi}^{int}} = \frac{\sum_l \alpha_l \Phi_l^{int}}{\bar{\Phi}^{int}}, \quad (2)$$

where Φ_l^{int} is the l th term in the multipole expansion at time t of interest, and α_l characterizes the increase in Φ_l^{int} over the previous crossing time; i.e. $\alpha_l = 0$ if the particular multipole does not increase, and $\alpha_l = 1$ if the multipole term is zero at time $t - t_{cross}$ and non-zero at t . For our discussion we will consider a spherical region positioned at the center of mass[¶] and thus we do not require the azimuthal terms in the multipole expansion – although our general argument does not depend sensitively on the shape of the aperture used to compute the moments. Since the $l > 0$ terms are not spherically symmetric, we average Φ_l^{int} over the spherical surface of radius r and denote it by $\langle \Phi_l^{int} \rangle$. Actually we average $\langle \Phi_l^{int} \rangle^2$ because $\langle \Phi_l^{int} \rangle = 0$ for $l > 0$.

Because we cannot observe a cluster for the duration of a crossing time, let us approximate equation (2) at the time t of interest. First, in the denominator we set $\bar{\Phi}^{int} \approx \Phi^{int}$ which is accurate to within a factor of 2, and set $\Phi^{int} \approx \Phi_0^{int}$, since the monopole term dominates the higher order terms for all reasonable cases. For a relaxed, smooth cluster the $l > 0$ ratios $\langle \Phi_l^{int} \rangle^2 / \langle \Phi_0^{int} \rangle^2$ are substantially smaller than for a cluster with subclumps that are a considerable ($\gtrsim 20\%$) fraction of the total mass (Buote & Tsai 1995)^{||}.

clusters formed in N-body simulations (e.g. Tormen, Bouchet, & White 1997).

[¶] The center of mass can be defined within the sphere of radius r through iteration.

^{||} Buote & Tsai actually discuss circularly averaged moments of

As a result, we may approximate equation (2) by setting $\alpha_l = 1$ for the $l > 0$ terms^{★★}. Making these substitutions we arrive at,

$$\frac{\langle (\Delta \Phi^{int})^2 \rangle}{\langle (\bar{\Phi}^{int})^2 \rangle} \approx \left(\frac{\Delta M}{\bar{M}} \right)^2 + \sum_{l>0} \frac{\langle (\Phi_l^{int})^2 \rangle}{\langle (\Phi_0^{int})^2 \rangle}, \quad (3)$$

which states that the fractional increase in the rms spherically averaged potential over a crossing time is approximately the fractional increase in the mass and the increases in the ratios of the rms spherically averaged higher order multipoles to the monopole added in quadrature. Violent relaxation (Lynden-Bell 1967) is the key process driving the elimination of large potential fluctuations. It operates on a timescale of $\sim 1 - 2$ crossing times and proceeds independently of the masses of the constituents in accordance with our picture of the morphological evolution of clusters stated above.

Hence, equation (3) is a definition of the dynamical state of a cluster and could have been the starting point of our discussion^{††}. By the nature of the multipole expansion, we see that only the low order moments are important for characterizing the dynamical state, with the monopole term being most important^{‡‡}. As a result, the possible long-term survival of the dense, compact cores of subclusters, which contribute mostly to the higher order moments, does not affect the shorter relaxation timescale of the low order moments most relevant to the dynamical state. (The implications of this property are discussed in §§5 and 6.)

2.2 Observational Consequences

The fractional change in the monopole, $\Delta M / \bar{M}$, cannot be directly observed over a relaxation time. However, our premise that the amount of accreted mass over the previous relaxation timescale determines the amount of substructure (or non-ellipsoidal distortions) requires that the monopole change be strongly correlated with the change in the low order terms, which are approximately the ratios, $\langle (\Phi_l^{int})^2 \rangle / \langle (\Phi_0^{int})^2 \rangle$, defined at the epoch under consideration. What is the nature of this correlation and, more importantly, how may $\Delta M / \bar{M}$ be inferred from cluster observations?

the projected potential which replace the cluster mass density with toy models of the X-ray surface brightness of clusters. Nevertheless, the qualitative features apply when the mass is used as shown §4 of Tsai & Buote (1996).

^{★★} This approximation implies that $\langle (\Delta \Phi^{int})^2 \rangle / \langle (\bar{\Phi}^{int})^2 \rangle \neq 0$ for virialized clusters because the even- l moments, though small in relation to clusters with considerable substructure, are non-zero in general for ellipsoidal masses.

^{††} For alternative indicators of the dynamical state of a cluster see Zaroubi, Naim, & Hoffman (1996) and Natarajan, Hjorth, & van Kampen (1997).

^{‡‡} Our formulation is a twist on the argument of Richstone et al. (1992) who computed the fraction of present-day clusters which “collapsed” over the previous relaxation time. This fraction is then interpreted as the “frequency of substructure” in the present cluster population. In our case, for an individual cluster the fractional accreted mass over the relaxation time approximately determines the importance of substructure in the cluster and thus its dynamical state.

For observations of clusters it is convenient to work with the projected potential, Ψ^{int} , and its circularly averaged (over radius R) multipole ratios, $\langle(\Psi_m^{int})^2\rangle/\langle(\Psi_0^{int})^2\rangle$. For the $m > 0$ terms it is unclear how to relate a measured $\langle(\Psi_m^{int})^2\rangle/\langle(\Psi_0^{int})^2\rangle$ to the multipole ratios in three-dimensions. However, the fractional change of the monopoles in 2-D and 3-D are comparable if the fractional accreted masses within the 2-D and 3-D regions are comparable. That is, let us again consider our prototype case where the 3-D region is a sphere of radius r defined at its center of mass. The corresponding 2-D region is the circle of radius $R = r$ resulting from the projection along its symmetry axis of the cylinder which encloses the sphere at its center. So long as the extra accreted mass in the portion of the cylinder outside the sphere does not contribute much to the total fractional accreted mass of the cylinder, then the 2-D and 3-D fractional monopole changes will be similar.

Hence, $\Delta\Phi_0^{int}/\bar{\Phi}_0^{int} \cong \Delta\Psi_0^{int}/\bar{\Psi}_0^{int}$ for projected radii containing a sizeable fraction of the total cluster mass. (An appropriate minimum radius can be determined from N-body simulations.) If we now consider the 2-D analogue of equation (3), then the correspondence of the 2-D and 3-D monopole changes coupled with the arguments made in the preceding section indicate that $(\Delta M/\bar{M})^2$ (3-D) should be strongly correlated with $\langle(\Psi_m^{int})^2\rangle/\langle(\Psi_0^{int})^2\rangle$, which are themselves easily computable observables of the cluster density distribution (Buote & Tsai 1995). For observations of an individual cluster this correspondence assumes that projection does not smear out the structure; e.g. axisymmetric clusters are viewed edge-on. Later in this section we discuss how to deal with projection effects.^{§§}

Three dimensional N-body simulations can explicitly quantify the relationship between $\Delta M/\bar{M}$ and $\langle(\Psi_m^{int})^2\rangle/\langle(\Psi_0^{int})^2\rangle$. There is reason to believe that this relationship will be very tight for small m and mostly independent of Ω_0 . For clusters observed with *ROSAT* (Buote & Tsai 1996) and those formed in both dissipationless (BX; Thomas et al. 1997) and dissipational N-body simulations (Tsai & Buote 1996), the ratios, $\langle(\Psi_m^{int})^2\rangle/\langle(\Psi_0^{int})^2\rangle$, are strongly correlated for the first few m – in fact the logarithms of these ratios are essentially proportional to each other ¶¶. We henceforth adopt the simplified notation $P_m/P_0 \equiv \langle(\Psi_m^{int})^2\rangle/\langle(\Psi_0^{int})^2\rangle$ used by these other studies.

Tsai & Buote (1996) studied these correlations in detail for both the X-ray surface brightness maps and the projected masses of six clusters formed in the N-body / hydrodynamical simulation of Navarro, Frenk, & White (1995). These correlations can be understood as tracks followed by clusters as they evolve via mergers and subsequent relaxation from infancy to quasi-virialized states (see Figure 6 of Tsai & Buote and §5.1 of Buote & Tsai 1996). For the larger values of P_m/P_0 (corresponding to the least relaxed clusters)

the $m = 2, 3, 4$ ratios are tightly correlated and are very nearly proportional to each other.

The scatter in these correlations is largest for the smallest values of P_m/P_0 as a result of projection effects. The smallest values of P_m/P_0 correspond to either relaxed, single-component clusters or to clusters with substructure smeared out by the act of projecting along the line of sight; e.g. a bimodal cluster being viewed along the merger axis. Thus, to minimize the projection effects the correlations between the low order P_m/P_0 (particularly for $\log_{10} P_2/P_0$ versus $\log_{10} P_4/P_0$) can be defined accurately for the larger values of P_m/P_0 where the scatter is low (see, e.g., Figure 3 of Buote & Tsai 1996, Figure 4 of BX, and Figure 9 of Thomas et al. 1997.) Moreover, the approximation $\alpha_l \equiv 1$ in equation (3) is most rigorously satisfied for these largest multipole ratios.

The shapes of these correlations do not show significant differences as a function of Ω_0 or $\lambda_0 = 1 - \Omega_0$ (BX), although Thomas et al. (1997) note that the $\log_{10} P_2/P_0$ versus $\log_{10} P_4/P_0$ correlation is tighter for the $\lambda_0 = 0$ models. Since these correlations are expected to apply as well to $\Delta M/\bar{M}$ (3-D), we may write,

$$\log_{10} \left(\frac{\Delta M}{\bar{M}} \right)^2 = c_m \log_{10} \frac{P_m}{P_0} + d_m, \quad (4)$$

where c_m and d_m are the linear coefficients which should be largely independent of Ω_0 and, for best accuracy, should be determined from fits to the largest values of $\log_{10} P_m/P_0$. By quantifying the c_m and d_m with N-body simulations we may infer $\Delta M/\bar{M}$ from observations of P_m/P_0 for a large sample of clusters and thus measure the value of Ω_0 ¶¶¶. (Another advantage of writing the expected correlations in terms of logarithms is that BX found that the means of the $\log_{10} P_m/P_0$ ($m = 2, 3, 4$) distributions of N-body clusters are influenced primarily by Ω_0 whereas the variances are affected mostly by the power spectrum of density fluctuations; i.e. the influence of the power spectrum may be largely circumvented by examining the means of the logarithmic distributions.)

Measurements of P_m/P_0 for clusters may be obtained from either gravitational lensing or X-ray data (for a discussion see §2 of Buote & Tsai 1995)***. Since gravitational lensing measures the projected mass directly, the coefficients c_m and d_m can be quantified by dissipationless simulations which is an advantage over X-ray data. However, the projection of the mass in simulated clusters appears to lead to smaller measured variations in P_m/P_0 than does the X-ray surface brightness (see §4 of Tsai & Buote 1996), and thus the larger dynamic range afforded by X-ray maps probably indicates a greater sensitivity to Ω_0 . This larger dynamic range occurs because for unrelaxed clusters the X-ray emitting gas approximately traces the mass but its emission is more responsive to density fluctuations since it goes as ρ_{gas}^2 . In the other limit, when the gas is in hydrostatic equilibrium the emission traces the potential for arbitrary temperature

§§ We show in §5.2.1 that the $\langle(\Psi_m^{int})^2\rangle/\langle(\Psi_0^{int})^2\rangle$ obtained from the N-body simulations of BX agree reasonably well with our calculations for $\Delta M/\bar{M}$.

¶¶ Again, although most of the references listed have focused on moments of the X-ray surface brightness, Tsai & Buote (1996) showed that taking moments of the mass gives very consistent results.

¶¶¶ A minimum of about 20 clusters appears to be required to distinguish between CDM models with $\Omega_0 = 1$ and $\Omega_0 = 0.3$ (Thomas et al. 1997).

*** Another route to observations is via cooling flows (e.g. Fabian 1994), where the cooling-flow rate should be *anti-correlated* with $\Delta M/\bar{M}$ (Buote & Tsai 1996)

gradient (§3.1 of Buote & Canizares 1994; §5.1 of Buote & Canizares 1996) and is thus smoother and rounder than the mass (see §2.3.1 of BX for a detailed discussion).

2.3 Present Application

Presenting a constraint on Ω_0 by obtaining the coefficients c_m and d_m (equation 4) from N-body simulations for comparison to observations is beyond the scope of the present paper. Instead we prefer to focus on the *differences* between CDM models with different Ω_0 since the differences in $\Delta M/\bar{M}$ can be related to differences in P_m/P_0 without knowledge of the as yet unknown coefficients d_m and by taking $c_m \approx 1$ as suggested by the $\log_{10} P_m/P_0$ correlations. For this task we can compute the quantity $\Delta M/\bar{M}$ using a spherical model for a cluster which has the significant advantages of being simpler conceptually and considerably less intensive computationally than three-dimensional N-body simulations. In this way we can gain physical insight into the morphological evolution of clusters in different cosmologies and rapidly explore the interesting parameter space to aid analysis of future three dimensional simulations and observations.

Of course, a spherical model is only an idealization, but the radial density profiles seen in three dimensional N-body simulations agree well with simple spherical accretion models (e.g. Navarro, Frenk, & White 1995; Anninos & Norman 1996; also see §5.1 of this paper). By using a spherical model we in essence compute a mean value of $\Delta M/\bar{M}$, whereas in a more realistic model the non-spherical nature of the merging process will induce fluctuations in $\Delta M/\bar{M}$ depending on how the mass is distributed in clumps during a merger. However, for studying the dependence of $\Delta M/\bar{M}$ on Ω_0 , the mean value should be sufficient since BX showed that it is primarily Ω_0 which determines the means of the distributions of P_m/P_0 for clusters formed in three-dimensional N-body simulations. We therefore adopt a spherical model for our present investigation.

3 COMPUTATION OF $\Delta M/\bar{M}$

3.1 Peaks formalism

It is our intention to work within the standard framework wherein small density inhomogeneities in the early universe grow by gravitational instability into the galaxy clusters that we see today. We restrict our discussion to the case where these initial density fluctuations are described by a gaussian random field, and, in particular, that the sites where clusters form are determined by high peaks in this perturbation field (Bardeen et al. 1986, hereafter BBKS). With these assumptions the average initial density profile around such high peaks is specified by the power spectrum of density fluctuations, $P(k)$. (For similar presentations of the following see Ryden & Gunn 1987, Ryden 1988, Hoffman 1988, and especially Lilje & Lahav 1991.)

The spherical accretion model (see §3.2) only depends on the density through the initial cumulative density contrast, $\bar{\delta}_i(x)$, defined at comoving position x at initial time t_i . The initial cumulative density contrast around a high peak in a gaussian random field is (BBKS),

$$\bar{\delta}_i = \left(\nu - \frac{\gamma\theta}{1-\gamma^2} \right) \frac{\bar{\xi}}{\sigma_0} - \frac{\theta}{1-\gamma^2} \frac{\bar{\nabla}^2 \xi}{\sigma_2}, \quad (5)$$

where $\gamma \equiv \sigma_1^2/(\sigma_2\sigma_0)$ and the spectral moments are defined by,

$$\sigma_\mu^2 = \frac{1}{2\pi^2} \int P(k) k^{2+2\mu} dk, \quad (6)$$

with the special case $\sigma_0^2 = \xi(0)$; the cumulative correlation function and its cumulative Laplacian are,

$$\bar{\xi} = \frac{1}{2\pi^2} \int P(k) k^2 w(kx) dk \quad (7)$$

$$\bar{\nabla}^2 \xi = \frac{-1}{2\pi^2} \int P(k) k^4 w(kx) dk, \quad (8)$$

(note: $\bar{\nabla}^2 \xi = \frac{3}{x} \frac{d\xi}{dx}$) where the top-hat filter is given by,

$$w(x) = \frac{3}{x^3} (\sin x - x \cos x). \quad (9)$$

The dimensionless parameter ν specifies the peak height, $\delta_i(0) = \nu\sigma_0$, and $\theta(\gamma, \nu)$ is given by equation (6.14) of BBKS with the asymptotic behavior $\theta \rightarrow 0$ as $\nu \rightarrow \infty$. Thus, for high peaks $\bar{\delta} \approx \nu\bar{\xi}/\sigma_0$. The peak only dominates the collapse in its vicinity which we take to be defined as the region where $\bar{\delta}_i \leq \sqrt{(\Delta\bar{\delta}_i)^2}$, where the variance in $\bar{\delta}_i$ is (BBKS),

$$(\Delta\bar{\delta}_i)^2 = \sigma_M^2 - \frac{1}{1-\gamma^2} \left[\frac{\bar{\xi}^2}{\sigma_0^2} + \frac{\bar{\nabla}^2 \xi}{\sigma_2} \left(2\gamma \frac{\bar{\xi}}{\sigma_0} + \frac{\bar{\nabla}^2 \xi}{\sigma_2} \right) \right], \quad (10)$$

where,

$$\sigma_M^2(x) = \frac{1}{2\pi^2} \int P(k) w^2(kx) k^2 dk, \quad (11)$$

is the mass variance in spheres of comoving radius x .

We do not consider secondary perturbations arising from non-sphericity and random velocities (BBKS) discussed by Ryden & Gunn (1987) and Ryden (1988) in the context of galaxy-sized halos. Such perturbations cause fluctuations in the collapse time of matter around the peak, though we do not expect angular momentum to play a dominant role in the formation of clusters since they are not observed to rotate appreciably. At any rate, uncertainties of this variety that affect the collapse time are related to our ignorance of the precise relaxation timescale over which low-order potential fluctuations are erased, the uncertainties of which we expect to dwarf those of the secondary perturbations. (We discuss this issue further in the next section.)

For our calculations we define the initial epoch to be at recombination, $z_i \equiv 1300$, though our results differ negligibly for any $z_i \gtrsim 50$. In practice we compute $\bar{\delta}_i$ by first evaluating $\bar{\delta}_0$, the cumulative density contrast extrapolated to the present using linear theory, by normalizing the linear power spectrum at $z = 0$ (see §4). Then $\bar{\delta}_i$ is computed from $\bar{\delta}_0$ assuming linear growth, for which we use the convenient approximation of Carroll, Press, & Turner (1992) for a universe with matter density parameter Ω and density parameter, λ , due to a cosmological constant.

3.2 Spherical accretion model

We evolve the initial cluster density distribution determined by the peaks formalism to a final state using the spherical

accretion model^{***}. It will now prove convenient to work in proper coordinates, $r = ax$, where $a(t)$ denotes the expansion factor at time t . For arbitrary Ω_0 and a monotonically decreasing density profile, the spherical collapse model (e.g. Peebles 1980; Padmanabhan 1993; Sahni & Coles 1995) exactly describes the expansion of spherical shells out to their maximum radius (“turn around”). (In the Appendix we give the equations for the zero-curvature universe with a cosmological constant $\lambda_0 = 1 - \Omega_0$.) After the shell reaches maximum expansion, it collapses and crosses the orbits of other shells at which point the spherical model no longer accurately describes the motion of the shell. If one restricts the solutions to those that are self-similar, then exact solutions may be found (Fillmore & Goldreich 1984; Bertschinger 1985). For the general case, however, methods must be used which specifically treat the interactions between the shells. The standard method to do this is with N-body simulations (e.g. Sigurdsson, Hernquist, & Quinlan 1995; Thoul & Weinberg 1995).

Another approach is to consider the growth of a density peak by computing the orbit of an infalling shell in the potential generated by the previously collapsed matter (Gunn 1977; Ryden & Gunn 1987 – also see Blumenthal et al. 1986). If the infalling shell induces only a small change in this potential, then the shell’s orbit may be computed using the adiabatic approximation. The accuracy of this approximation is determined by the number of shells, N , used to divide up the mass distribution. Typically, only for the first few (innermost) shells does the potential change substantially. For large N (~ 100) the errors associated with this approximation have a negligible effect on shells at radii that are of interest to our present study.

To construct a cluster using the adiabatic method (see Ryden & Gunn 1987) one begins with a core mass distribution, taken to correspond to the scale over which the power spectrum is smoothed (see §4). The details of the shape of this core have no tangible effect on the shells at radii of interest. We consider now the first mass shell orbiting in the potential generated by the core mass. The energy per unit mass of the shell is an integral of the motion and is equal to the potential at the maximum radius of the orbit. More generally, we may write for a shell n falling into the potential, Φ_n , generated by the mass of the previous $n - 1$ shells plus the core as,

$$E_n = \Phi_n(r_m^n) \quad (12)$$

$$= \frac{1}{2} \left(\frac{dr}{dt} \right)^2 + \Phi_n(r), \quad (13)$$

where r_m^n is the (proper) maximum radius of the n th shell. For the first shell we have $\Phi_1 = \Phi_c$, the potential generated by the core mass. The amount of mass a shell contributes within a radius interval dr is determined by the fractional amount of time that it spends passing through dr during its orbit. The amount of time the shell spends within a radius interval dr is just $dt = dr/v_r$, and thus the fractional amount of time, which is just the probability of finding the shell within dr , is,

$$P_n(r)dr = \frac{dr/v_r^n}{\int_0^{r_m^n} dr/v_r^n}, \quad (14)$$

and $v_r^n = |dr/dt|$ is the radial speed of shell n , which for the first shell is,

$$v_r^1 = \sqrt{2[E_1 - \Phi_c(r)]}. \quad (15)$$

Hence, the combined mass of the core and the first shell may be written generally,

$$M_n(r) = M_{n-1}(r) + M_{sh} \int_0^r P_n(r)dr, \quad (16)$$

where M_{sh} is the total mass of the shell and $M_0 = M_c$.

The next shell is added analogously to the first by computing its energy, E_2 , in the potential, Φ_2 , generated by mass, M_1 , and results in a new mass, M_2 . Now, however, the first shell sees a different mass due to the overlapping orbit with the second shell. If the potential change is small, then the energy of the first shell decreases, but since the radial action,

$$j_r = \int_0^{r_m} v_r dr, \quad (17)$$

is conserved, the effect is to reduce the maximum radius of the orbit of the first shell (Gunn 1977)^{***}. Hence, when the second shell is added, j_r is recomputed for the first shell in the potential generated by the mass M_2 . Then r_m^1 is adjusted so that the action equals its initial value. For an adiabatic change in the potential, the new value of r_m is approximately,

$$r_m^{new} = r_m^{old} \frac{j_r^{old}}{j_r^{new}}, \quad (18)$$

where $j_r^{new} = \int_0^{r_m^{old}} v_r^{new} dr$, with v_r^{new} computed using the potential incorporating the new overlapping shell – for the case under consideration, the potential generated by the mass M_2 . Equation (18) can be iterated by computing a new j_r^{new} using r_m^{new} as the new upper limit in the integral until desired precision in r_m^{new} is achieved. Once the radius of the first shell has been modified to reflect the addition of the second shell, a new value of M_2 is computed.

(At this point one should in principle repeat this procedure for the first and second shells until r_m^1 and M_2 change within desired tolerances. However, corrections of this type are negligible when the initial potential change is small, which applies as n becomes large. We neglect these higher order corrections.)

This adiabatic addition of shells continues until all of the collapsed shells have been incorporated into the aggregate virialized cluster. In general not all of the mass bound to the peak has collapsed at the redshift of interest, say z . We define the last collapsed shell to be that which has just reached $r = 0$ at redshift z . We compute this directly by integrating dr/v_r for each shell rather than estimating the collapse time as $2t_m$. For the shells that are bound to the

^{***} For a discussion of some of the caveats associated with this type of approach see Lilje & Lahav (1991) and Bernardeau (1994).

^{***} For the first few shells the radii can actually increase because the density profile changes drastically in shape with the addition of each new shell; i.e. the addition of the first few shells is not really adiabatic if the shell mass is comparable to the core mass.

peak but uncollapsed at z , we let them fall into the cluster potential and assign them to their infall radii at z . Note that Ryden & Gunn (1987; Ryden 1988) did not treat the uncollapsed matter while Hoffman (1988) allowed all of the matter to collapse.

After building the cluster mass distribution at the epoch of interest, we evaluate the crossing time which we take to be,

$$t_{cross} \equiv 2 \frac{R_{1/2}}{\sigma}, \quad (19)$$

where $R_{1/2}$ is the half-mass radius and σ is the one-dimensional (radial) velocity dispersion computed using the virial theorem. Next, we construct the cluster mass distribution at the earlier time, $t - t_{cross}$. Finally, we evaluate the fractional amount of mass accreted within a radius r over the time interval $(t - t_{cross}, t)$,

$$\frac{\Delta M}{\bar{M}} = \frac{M(r, t) - M(r, t - t_{cross})}{\frac{1}{2}[M(r, t) + M(r, t - t_{cross})]}, \quad (20)$$

where ΔM is the mass difference and \bar{M} is the average mass. As we show in §5, the value of $\Delta M/\bar{M}$ is quite sensitive to the time interval $(t - t_{cross}, t)$ used to represent the relaxation timescale. We need only consider a relaxation timescale that is $\sim 1 - 2$ crossing times since, as mentioned in §2, we are interested only in substructure contributing to fluctuations in the low order moments of the gravitational potential.

However, even the relatively modest range of $\sim 1 - 2$ crossing times causes sufficiently large changes in $\Delta M/\bar{M}$ to make further refinements to our spherical accretion model unwarranted; e.g. the secondary perturbations due to non-sphericity and angular momentum discussed in §3.2, initial peculiar velocities (Bartelmann et al. 1993), or a small (and difficult to precisely define) drag force due to substructure (Antonuccio-Delogu & Colafrancesco 1994; Del Popolo & Gambera 1996). Each of these effects either increase or decrease the collapse times for the mass shells, of which the combined effect is unclear, and such uncertainties should be largely absorbed into the $\sim 1 - 2$ crossing time range assumed for the relaxation timescale (as is the uncertainty in our specific definition of t_{cross} itself).

We now describe a quantity related to $\Delta M/\bar{M}$ which does not require following the detailed virialization process of the cluster. The mass shell that has just collapsed at the epoch of interest, t , reached maximum expansion approximately at a time, $t/2$. For a given peak height, we can invert the equation for the time at maximum expansion to obtain the initial radius of this shell. The mass enclosed by this shell is,

$$M(< r_i) = \frac{4\pi}{3} \rho_b(t_i) r_i^3 (1 + \bar{\delta}_i), \quad (21)$$

where r_i is the initial (proper) radius. Because at maximum expansion the shell has not yet crossed the orbits of other shells, the enclosed mass $M(< r_m) = M(< r_i)$, where r_m is the radius of maximum expansion. Let us denote this enclosed mass as $M_{ta}(t/2) \equiv M(< r_m)$. Analogously, we can estimate the mass that has collapsed at the time $t - t_{cross}$ by computing $M_{ta}([t - t_{cross}]/2)$. Hence, an estimate of the fractional collapsed mass accreted over the previous crossing time is,

$$\frac{\Delta M_{ta}}{\bar{M}_{ta}} = \frac{M_{ta}(t/2) - M_{ta}([t - t_{cross}]/2)}{\frac{1}{2}[M_{ta}(t/2) + M_{ta}([t - t_{cross}]/2)]}, \quad (22)$$

which is computed directly from the turn-around times for the mass shells and thus does not involve treating the detailed virialization process. (The crossing time in this case is taken to be a constant which is a good approximation for the clusters produced by the adiabatic treatment of virialization – see §5.2.1.) Comparing $\Delta M_{ta}/\bar{M}_{ta}$ to $\Delta M/\bar{M}$ allows us to assess the impact of incorporating the virialization process into our calculations.

4 COSMOLOGICAL MODEL PARAMETERS

We consider power spectra appropriate for hierarchical clustering, in particular CDM and power-law $P(k)$. We take the linear CDM power spectrum according to BBKS,

$$P(k)_{CDM} \propto k \left(\frac{\log(1 + 2.34q)}{2.34q} \right)^2 \times [1 + 3.89q + (16.1q)^2 + (5.46q)^3 + (6.71q)^4]^{-1/2}, \quad (23)$$

where we have assumed the scale-invariant form ($P(k) \propto k$) for the primordial spectrum. The spectrum is expressed in terms of the parameter $q \equiv k/(h\Gamma)$, where the “shape parameter” is defined to be (Sugiyama 1995),

$$\Gamma \equiv \Omega_0 h \exp(-\Omega_B - \Omega_B \Omega_0^{-1}), \quad (24)$$

where Ω_B is the density parameter of baryonic mass. We adopt as our standard the value $\Omega_B h^2 = 0.016$ (Copi et al. 1995) consistent with Big Bang Nucleosynthesis. However, we also examine models with the larger value inferred from the X-ray gas content in clusters, $\Omega_B h^{-3/2}/\Omega_0 = 0.05$ (White & Fabian 1995).

We use the shape parameter to set the value of h for the CDM models ($H_0 = 100h \text{ km s}^{-1} \text{ Mpc}^{-1}$). Viana & Liddle (1996) determine 95% confidence limits $\Gamma \approx 0.2 - 0.3$ using the galaxy autocorrelation function data from Peacock & Dodds (1994). We slightly expand this range to $\Gamma = 0.15 - 0.35$ and construct a linear relation with Ω_0 such that $\Gamma = 0.15$ for $\Omega_0 = 0.2$ and $\Gamma = 0.35$ for $\Omega_0 = 1$. This function $\Gamma(\Omega_0, h)$ – at fixed Ω_B – allows us to determine a value of h as a function of Ω_0 consistent with current data (though see Peacock 1997) with the slightly expanded range chosen to keep the values of $h \approx 0.45 - 0.85$ within reasonable observational limits (e.g. Fukugita, Hogan, & Peebles 1993).

To eliminate the divergence of $P(k)_{CDM}$ at small wavelengths we follow the standard procedure and mathematically smooth the power spectrum with a gaussian filter, $P(k)_s \propto P(k)_{CDM} \exp(-k^2 l^2/2)$, where l is the smoothing length in comoving coordinates. The mass contained within the gaussian filter is $M_s = (2\pi)^{3/2} \rho_b(l/\sqrt{2})^3$ at $z = 0$. Since we are interested in mass fluctuations of the size of clusters of galaxies, we choose $M_s = 10^{12} h^{-1} M_\odot$ which corresponds to the mass of a large galaxy at the present epoch, since structures with $M \lesssim M_s$ individually have a negligible contribution to the dynamical evolution of a cluster. The smoothing length corresponding to this M_s is $l = 0.86 \Omega_0^{-1/3} h^{-1} \text{ Mpc}$. For evaluating $\Delta M/\bar{M}$ at higher redshifts, we approximately account for the smaller masses of galaxies by reducing the smoothing mass according to,

$M_s(z) = M_s(0)/(1+z)$, which is just the self-similar accretion law $M \propto t^{2/3}$ (Bertschinger 1985). (The results we obtain for $\Delta M/\overline{M}$ in the next section are not overly sensitive to l .)

To normalize the smoothed CDM power spectrum we first set the value of $\sigma_8 = \sigma_M(8h^{-1}\text{Mpc})$, the linearly extrapolated rms mass fluctuation in spheres of radius $8h^{-1}\text{Mpc}$, to agree with the abundance of X-ray clusters at the present day ($z = 0$),

$$\begin{aligned}\sigma_8 &= 0.52\Omega_0^{(-0.46+0.10\Omega_0)} & \lambda_0 &= 0 \\ \sigma_8 &= 0.52\Omega_0^{(-0.52+0.13\Omega_0)} & \Omega_0 + \lambda_0 &= 1,\end{aligned}\quad (25)$$

where we have used the best-fit results of Eke, Cole, & Frenk (1996). We obtain σ_8 for higher redshifts using the same scaling relation for the density in §3.1. The number of clusters as a function of mass measures the amplitude of fluctuations in the mass on cluster scales (see, e.g., Frenk et al. 1990), whereas we require the amplitude of fluctuations in clusters (i.e. integrated over mass). In the peaks formalism, clusters are biased tracers of the mass distribution which may be accounted for by increasing the mass fluctuation amplitude by a bias factor (BBKS; Bardeen et al. 1987),

$$b_{clus} \equiv \frac{\langle \tilde{\nu} \rangle}{\sigma_0} + 1, \quad (26)$$

where $\langle \tilde{\nu} \rangle$ is an average peak height of the model under consideration above some threshold ν_t . The cluster power spectrum is then, $P(k)_{clus} = b_{clus}^2 P(k)_{mass}$, where $P(k)_{mass}$ is the smoothed CDM power spectrum normalized using the above relation for σ_8 .

We evaluate b_{clus} in a manner similar to that described in Croft & Efstathiou (1994) (also see Efstathiou et al. 1992). First, we smooth the mass power spectrum with a gaussian of length $l = 5\sqrt{2}\Omega_0^{-1/3}h^{-1}\text{Mpc}$ and normalize to the above σ_8 . This smoothing length gives appropriate cluster masses over a wide range of cluster abundances (Croft & Efstathiou 1994). We focus our attention on clusters with masses exceeding $3.5 \times 10^{14}h^{-1}M_\odot$ corresponding to an abundance of $\sim 1 \times 10^{-5}\text{Mpc}^{-3}$ for typical CDM models (see Figure 1 of White, Efstathiou, & Frenk 1993). By requiring that the number density of peaks in our model match this cluster abundance, we specify the peak threshold, ν_t , and thus $\langle \tilde{\nu} \rangle$. For CDM models with $\Omega_0 = 0.2 - 1$ we obtain bias parameters $b_{clus} \approx 1 - 3.5$.

We also consider models with power-law power spectra, $P(k)_{pl} \propto k^n$, with n ranging from 0 to -2. Because $P(k)_{pl}$ also diverges for small wavelengths we smooth it in the same manner as $P(k)_{CDM}$. We normalize the smoothed power spectrum in the same manner as done for the CDM spectrum and compute appropriate bias factors. This is feasible because the σ_8 - Ω_0 relationship given above is very insensitive to the shape of the power spectrum (e.g. White et al. 1993).

After choosing a power spectrum and specifying the remaining model parameters, we construct clusters having masses spanning the range $(0.35-3) \times 10^{15}h^{-1}M_\odot$. However, in the peaks formalism the size of an over-density region is specified by the peak height, ν , rather than the mass. When examining clusters at $z > 0$, we use ν determined at $z = 0$; e.g. for a $1 \times 10^{15}h^{-1}M_\odot$ cluster defined at $z = 0$, we study its progenitor at $z > 0$ which has the same ν but smaller mass. Note that whenever we quote cluster masses in the

next section we refer to the actual mass computed from the full spherical model calculation within $r = 1.5h^{-1}\text{Mpc}$.

5 RESULTS

5.1 Mass profiles at $z = 0$

Although not the focus of our present study, considerable literature exists on the theoretical density profiles of clusters. Hence, to place our model clusters in context, we briefly summarize the properties of the cluster mass profiles obtained from the spherical accretion model at $z = 0$ for a CDM power spectrum. A more detailed discussion of the density profiles will appear in a separate paper (Buote 1997).

In Figure 1 we display the density and mass profiles of clusters with mass $\sim 7 \times 10^{14}h^{-1}M_\odot$ formed in models with $\Omega_0 = 0.2, 1$. Only the virialized matter is shown for the density profiles since the infalling shells contribute (formally) infinite density spikes at their locations. We express the radii in terms of r_{200} , the radius where the mean cluster density is 200 times the background value: $r_{200} = 1.63 \times 10^{-5}(M/h^{-1}M_\odot)^{1/3}\text{Mpc}$ (e.g. Navarro, Frenk, & White 1997). For the clusters shown, $r_{200} \cong 1.5h^{-1}\text{Mpc}$.

Without the infalling material $\rho(r)$ is virtually identical within r_{200} for both $\Omega_0 = 0.2, 1$. For $r \lesssim 0.2r_{200}$ the virialized portions of the clusters approximately follow the self-similar profile $\rho \sim r^{-9/4}$ (Bertschinger 1985) and steepen to $\rho \sim r^{-2.5}$ at larger radii $r \sim (1-1.5)h^{-1}\text{Mpc}$. When the infalling mass is included the behavior at small radii is largely unaffected, but at large radii the $\Omega_0 = 1$ profile becomes flatter than $\Omega_0 = 0.2$: $\rho \sim r^{-2.4}$ for $\Omega_0 = 1$ and $\rho \sim r^{-2.5}$ for $\Omega_0 = 0.2$ over radii $r \sim (0.5-1)r_{200}$ or $r \sim (0.75-1.5)h^{-1}\text{Mpc}$. For a given Ω_0 the profile shapes of clusters of different masses are essentially identical when expressed in terms of r_{200} .

The density and mass profiles appear to agree well with those produced in the three-dimensional N-body simulations of a standard CDM cosmology. The $\rho \sim r^{-9/4}$ dependence in the inner regions giving way to a steeper density profile matches the behavior found by Anninos & Norman (1996) in their detailed study of the effect of mass resolution on cluster density profiles. Moreover, the relative similarity of the density profiles for different masses and different values of Ω_0 agrees with the conclusions of Navarro et al. (1997), aside from the core regions ($r \lesssim 0.2r_{200}$) where Navarro et al. find $\rho \sim r^{-1}$.

5.2 $\Delta M/\overline{M}$

5.2.1 CDM: $z = 0$ ($\lambda_0 = 0$)

We begin our discussion by examining the results of $\Delta M/\overline{M}$ at $z = 0$ for CDM models with $\lambda_0 = 0$. At present we restrict our discussion to the case where the relaxation timescale equals t_{cross} . In Figure 2 we show the radial dependence of $\Delta M/\overline{M}$ for a couple of representative masses with $\Omega_0 = 0.2, 1$. The profiles of $\Delta M/\overline{M}$ are nearly constant, though there appears to be a slight ($\sim 10\%$) increase with radius for low-mass clusters when $\Omega_0 = 1$; i.e. the dynamical state, or degree of virialization, is not a strong function of radius within $1.5h^{-1}\text{Mpc}$. The slight increase of

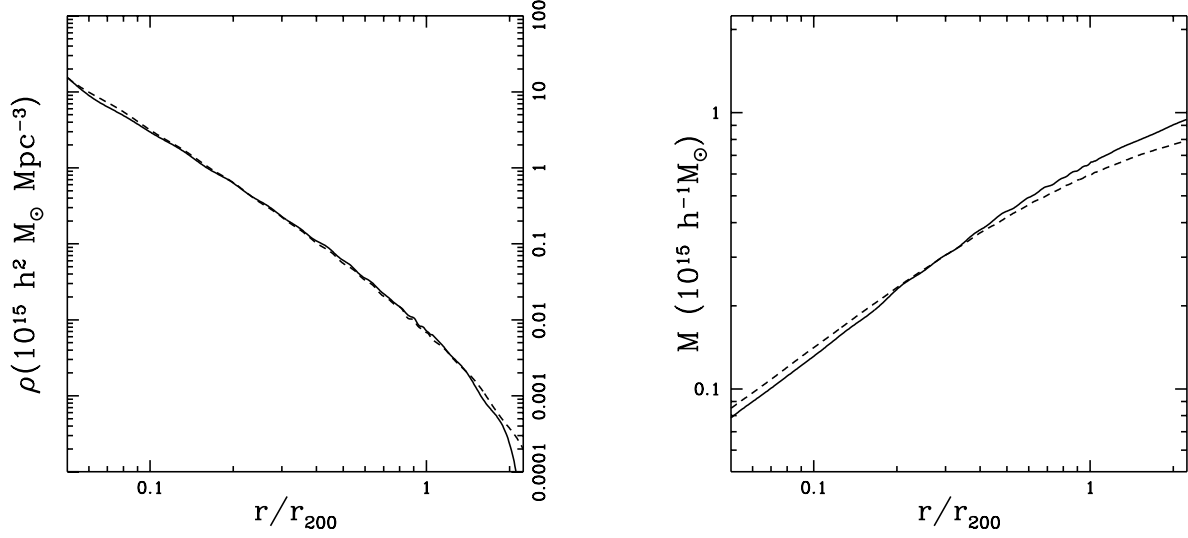


Figure 1. Density (left) and mass (right) profiles of $\approx 7 \times 10^{14} h^{-1} M_{\odot}$ clusters in CDM models with $\Omega_0 = 0.2$ (dashed) and $\Omega_0 = 1$ (solid). Only the contribution from virialized matter is shown for the density profiles while the mass profiles contain both the virialized and infalling mass.

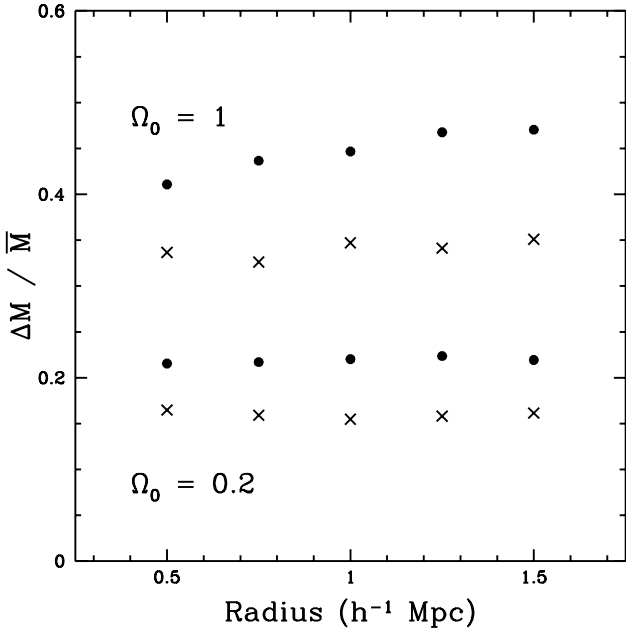


Figure 2. The radial profile of $\Delta M/\bar{M}$ at $z = 0$ for CDM models with $\Omega_0 = 0.2, 1$. Clusters with mass $\approx 3.5 \times 10^{14} h^{-1} M_{\odot}$ are shown as filled circles and those of mass $\approx 1.4 \times 10^{15} h^{-1} M_{\odot}$ by crosses. (These masses are approximately the values within a radius $1.5 h^{-1}$ Mpc.)

$\Delta M/\bar{M}$ with radius is reasonable since the amount of accreting mass becomes fractionally more important at larger radii, and models with larger Ω_0 have proportionally more accreting mass***.

*** The similar radial dependence of $\Delta M/\bar{M}$ for different masses also indicates that there is no conceptual advantage to focusing on a scaled radius like r_{200} .

To assess the reliability of $\Delta M/\bar{M}$ with respect to the simplifications of our model, we compare to the results of the N-body simulations of BX. However, BX analyzed the projection of ρ^2 and focused on the mean values of $\log_{10} P_m/P_0$ ($m = 2, 3$) of their N-body cluster samples, where $P_m/P_0 \equiv \langle (\Psi_m^{int})^2 \rangle / \langle (\Psi_0^{int})^2 \rangle$ (see §2). Although these properties prohibit a rigorous quantitative comparison of $\Delta M/\bar{M}$ to the BX results, we expect qualitative similarities. Henceforth we shall compare our results for $\Delta M/\bar{M}$ to the P_m/P_0 results obtained by BX with these caveats understood. For our comparison at hand, the nearly constant radial behavior of $\Delta M/\bar{M}$ is similar to P_m/P_0 , though the P_m/P_0 actually show a modest decrease with radius. This decrease in P_m/P_0 is expected because the properties of the multipole expansion dictate that higher order moments in the potential decay much more rapidly than the monopole with increasing distance from a mass concentration.

In Figure 3 we display $\Delta M/\bar{M}$ as a function of cluster mass (i.e. defined within $1.5 h^{-1}$ Mpc). The dependence of $\Delta M/\bar{M}$ on cluster mass is significant: for a given radius the more massive clusters tend to have smaller $\Delta M/\bar{M}$. This is a reflection of the shorter relaxation (crossing) times for the more massive clusters within a given radius. The slightly steeper dependence for the low mass clusters within the $1.5 h^{-1}$ Mpc aperture just reflects the slight increase with radius of $\Delta M/\bar{M}$ for $\Omega = 1$ models discussed above (see Figure 2).

Now we focus our attention on how $\Delta M/\bar{M}$ depends on Ω_0 . Since observations and N-body simulations give mean values averaged over a cluster sample, we average $\Delta M/\bar{M}$ over the mass function appropriate for our CDM models. Although the peaks formalism (BBKS) does not provide a well defined mass function, the analytic Press-Schechter (Press & Schechter 1974) mass function is convenient and a suitable approximation in many cases (Bond et al. 1991). For our averaging procedure we compute $\Delta M/\bar{M}$ for a few clusters spanning the mass range $(0.35 - 3) \times 10^{15} h^{-1} M_{\odot}$ and interpolate $\Delta M/\bar{M}$ for arbitrary M over that range. This func-

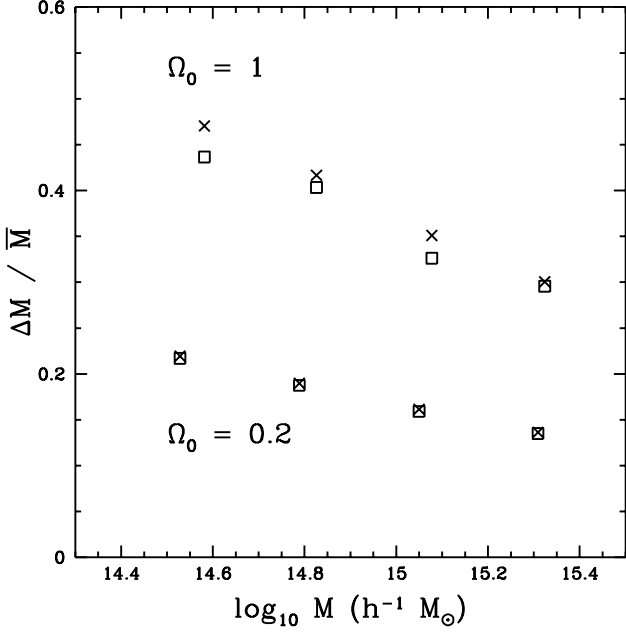


Figure 3. $\Delta M / \overline{M}$ evaluated for radii $r = 0.75h^{-1}$ Mpc (boxes) and $r = 1.5h^{-1}$ Mpc (crosses) as a function of total cluster mass within $1.5h^{-1}$ Mpc for $\Omega_0 = 0.2, 1$ CDM models at $z = 0$.

tion is then averaged over the Press-Schechter mass function using the approximations in Viana & Liddle (1996) for CDM models to yield the mass-averaged fractional accreted mass denoted by $\langle \Delta M / \overline{M} \rangle$.

In Figure 4 we display $\langle \Delta M / \overline{M} \rangle$ within $r = 1h^{-1}$ Mpc as a function of Ω_0 ($\lambda_0 = 0$). As expected, $\langle \Delta M / \overline{M} \rangle$ increases with increasing Ω_0 : $\langle \Delta M / \overline{M} \rangle \cong 0.46\Omega_0^{0.45}$ when averaged over the full mass range $(0.35 - 3) \times 10^{15}h^{-1}M_\odot$, and $\langle \Delta M / \overline{M} \rangle \cong 0.40\Omega_0^{0.50}$ when averaged over the smaller range $(0.7 - 3) \times 10^{15}h^{-1}M_\odot$ corresponding to more massive clusters. The slight variation of the exponent of Ω_0 as a function of mass range is the result of the mass averaging – we find that $\Delta M / \overline{M} \propto \Omega_0^{0.47}$ applies essentially over the full mass range $(0.35 - 3) \times 10^{15}h^{-1}M_\odot$. Given the results of Figures 2 and 3, it is not surprising that there is little advantage in going to larger radii as the greatest increase is seen within $r = 1.5h^{-1}$ Mpc for the least massive clusters for which we obtain the marginally steeper dependence $\langle \Delta M / \overline{M} \rangle \cong 0.47\Omega_0^{0.47}$ averaged over the full mass range.

To determine the relationship between this $\sim \Omega_0^{1/2}$ dependence and the turn-around times of the mass shells we compare these results to $\Delta M_{ta} / \overline{M}_{ta}$. Setting $t_{cross} = 0.14/H_0$ (see below) we compute $\Delta M_{ta} / \overline{M}_{ta}$ as a function of collapsed mass at $z = 0$. In Figure 5 we display $\Delta M_{ta} / \overline{M}_{ta}$ as a function of Ω_0 for a collapsed mass $7 \times 10^{14}h^{-1}M_\odot$. In agreement with the behavior of $\Delta M / \overline{M}$, we find $\Delta M_{ta} / \overline{M}_{ta} \propto \Omega_0^{0.48}$ which is essentially independent of mass over the full range $(0.35 - 3) \times 10^{15}h^{-1}M_\odot$. The normalization of $\Delta M_{ta} / \overline{M}_{ta}$, however, is $\sim 40\%$ smaller: $\Delta M_{ta} / \overline{M}_{ta} \cong 0.28\Omega_0^{0.48}$ versus $\Delta M / \overline{M} \cong 0.43\Omega_0^{0.47}$ for $7 \times 10^{14}h^{-1}M_\odot$. The close agreement between $\Delta M / \overline{M}$ and $\Delta M_{ta} / \overline{M}_{ta}$ indicates that the $\sim \Omega_0^{1/2}$ dependence is derived from the turn-around times of the mass shells. (This depen-

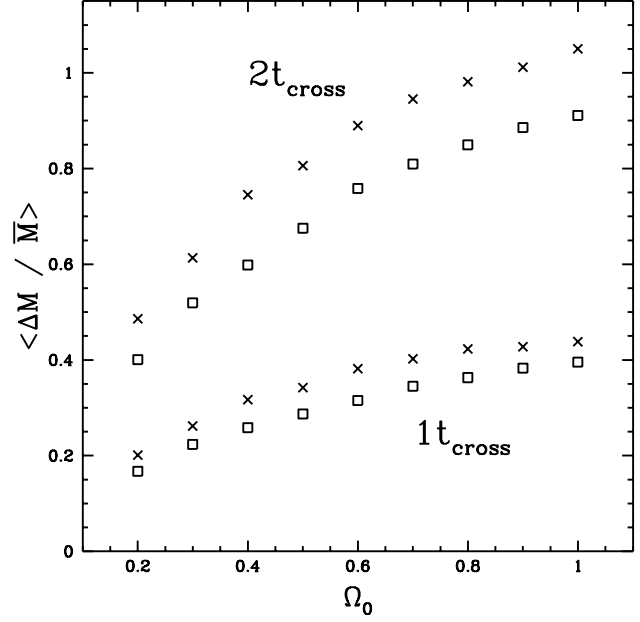


Figure 4. The mass-averaged fractional accreted mass evaluated for $r = 1h^{-1}$ Mpc at $z = 0$ for CDM models as a function of Ω_0 ($\lambda_0 = 0$). The crosses indicate a mass average over the full range $(0.35 - 3) \times 10^{15}h^{-1}M_\odot$, and the boxes indicate a lower limit of $7 \times 10^{14}h^{-1}M_\odot$. Relaxation timescales of 1 and 2 crossing times are shown.

dence is only weakly affected by the relaxation timescale – see below.)

We now compare $\langle \Delta M / \overline{M} \rangle$ to the N-body results of BX. In order to make the comparison more reasonable, let us consider $\log_{10} \langle (\Delta M / \overline{M})^2 \rangle$ within the $0.75h^{-1}$ Mpc aperture, for which our models give $\langle (\Delta M / \overline{M})^2 \rangle \cong 0.19\Omega_0^{0.81}$ over the full mass range. Let us consider the logarithmic difference of this quantity between a model with $\Omega_0 = 1$ and $\Omega_0 < 1$ and denote this shift by Δ . We can then write, $\Delta = -0.81 \log_{10} \Omega_0$. Setting $\Omega_0 = 0.35$ appropriate for BX (and $c_m = 1$, see §2.3), we obtain $\Delta = 0.4$, in pretty good agreement with $\Delta \sim 0.5$ obtained by BX considering that they analyzed ρ^2 in projection^{***}. This qualitative agreement with BX is reassuring on two accounts: (1) $\langle \Delta M / \overline{M} \rangle$, which represents the fractional increase in the monopole of the potential, clearly does correlate strongly with the next few low order moments; (2) our simple spherical accretion model is able to reasonably reproduce the differences in the means of cluster distributions generated by three-dimensional N-body simulations.

We may also compare $\langle \Delta M / \overline{M} \rangle$ to the results of Richstone et al. (1992) who apply the spherical collapse model to clusters of mass $10^{15}h^{-1}M_\odot$ arising from homogeneous density perturbations, which are assumed to form at the time equal to twice the turn-around time of the perturbation. Richstone et al. compute the quantity δF , the fraction of present-day clusters which formed within the last time

^{***} The projection of the dark matter in clusters appears to yield smaller variations in P_m/P_0 than does the projection of ρ_{gas}^2 (see §4 of Tsai & Buote).

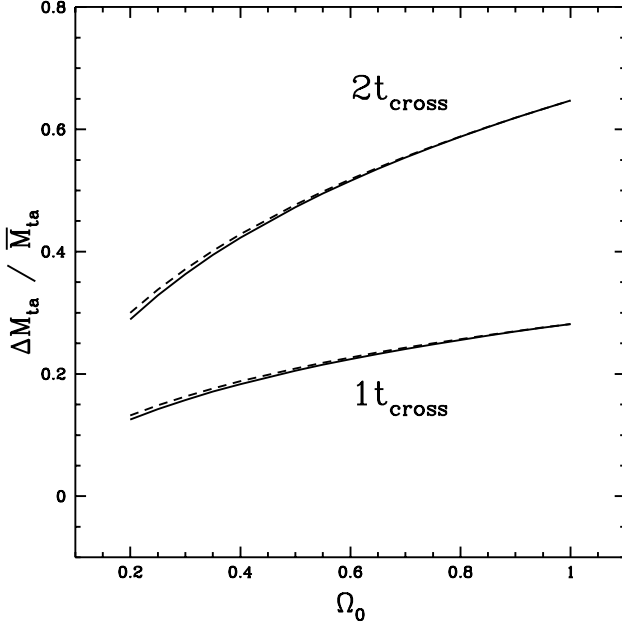


Figure 5. The fractional “collapsed” mass accreted over the previous relaxation time as a function of Ω_0 for CDM models at $z = 0$. The collapsed mass is approximately $7 \times 10^{14} h^{-1} M_\odot$ enclosed within a radius $1.5 h^{-1}$ Mpc. The solid lines indicate the $\lambda_0 = 0$ models, and dashed lines indicate $\Omega_0 + \lambda_0 = 1$ models. Relaxation timescales of 1 and 2 crossing times are shown where $t_{cross} \equiv 0.14/H_0$.

interval δt , as a function of Ω_0 and λ_0 . Consulting Figure 3 of Richstone et al. we see that $\delta F \sim \Omega_0$ for substructure survival time $\delta t = 0.1/H_0$ (a timescale similar to our $1t_{cross}$). (A similar dependence of δF on Ω_0 is seen in Figure 13 of Lacey & Cole 1993.)

Although δF is computed from the collapse times of density perturbations, it depends on these collapse times through the error function; i.e. $\langle \Delta M / \bar{M} \rangle$ and δF are qualitatively different in how they depend on the collapse times of shells and thus Ω_0 . In fact, we can repeat the exercise above for computing the mean shift between models with $\Omega_0 = 1$ and $\Omega_0 < 1$ by replacing $\langle \Delta M / \bar{M} \rangle$ with δF in which case we obtain $\Delta = -2 \log_{10} \Omega_0$. For $\Omega_0 = 0.35$, $\Delta = 0.9$ which is almost twice the mean shift found by BX. The significantly better agreement of the Δ predicted by $\langle \Delta M / \bar{M} \rangle$ over δF with the results of BX demonstrates that a much closer relationship exists between $\langle \Delta M / \bar{M} \rangle$ and P_m/P_0 than between δF and P_m/P_0 as would be expected.

The crossing times for the ($\lambda_0 = 0$) CDM models are not a strong function of mass or Ω_0 : $t_{cross} = (0.12 - 0.17)/H_0$ with a typical value $t_{cross} \cong 0.14/H_0 \cong 1.4 \times 10^9 h^{-1}$ yr. (The largest value corresponds to a mass $3.5 \times 10^{14} h^{-1} M_\odot$ for $\Omega_0 = 1$.) We show in Figure 4 the results for $\langle \Delta M / \bar{M} \rangle$ for the case where the relaxation timescale is set to $2t_{cross}$. Although the values of $\langle \Delta M / \bar{M} \rangle$ have approximately doubled, the power-law dependence on Ω_0 remains virtually unchanged: $\langle \Delta M / \bar{M} \rangle \cong 1.08 \Omega_0^{0.45}$ when averaged over the full mass range $(0.35 - 3.5) \times 10^{15} h^{-1} M_\odot$, and $\langle \Delta M / \bar{M} \rangle \cong 0.94 \Omega_0^{0.49}$ when averaged over the smaller range $(0.7 - 3) \times 10^{15} h^{-1} M_\odot$. This behavior is mirrored by $\Delta M_{ta} / \bar{M}_{ta}$

which maintains its $\Omega_0^{0.48}$ dependence for $2t_{cross}$ (Figure 5). (Note this same type of Ω_0 -dependence also applies for a relaxation timescale of $0.5t_{cross}$.)

A noticeable weakening of the dependence on Ω_0 occurs when the relaxation timescale is increased to $3t_{cross}$: $\langle \Delta M / \bar{M} \rangle \cong 1.71 \Omega_0^{0.35}$ when averaged over the full mass range $(0.35 - 3.5) \times 10^{15} h^{-1} M_\odot$, and $\langle \Delta M / \bar{M} \rangle \cong 1.61 \Omega_0^{0.45}$ when averaged over the smaller range $(0.7 - 3) \times 10^{15} h^{-1} M_\odot$. For a cluster that accretes an increasingly larger fraction of its current mass during the relaxation time, $\Delta M / \bar{M}$ approaches a value of 2 independent of Ω_0 . Because the smaller masses tend to have larger $\Delta M / \bar{M}$, their dependence on Ω_0 weakens more rapidly with redshift than the more massive clusters.

$\Delta M_{ta} / \bar{M}_{ta}$ is slower to respond to this effect. For $3t_{cross}$, $\Delta M_{ta} / \bar{M}_{ta} \cong 1.21 \Omega_0^{0.46}$ for a mass $3.5 \times 10^{14} h^{-1} M_\odot$. This becomes $1.80 \Omega_0^{0.39}$ at $4t_{cross}$ and approximately $2.09 \Omega_0^{0.17}$ at $5t_{cross}$. The departure of $\Delta M_{ta} / \bar{M}_{ta}$ from $\Delta M / \bar{M}$ indicates that the dynamical evolution depends more on the virialized structure of the cluster for large relaxation times, or equivalently for larger redshifts. (This effect is discussed in more detail in §5.2.3.)

For our current purposes the trend of $\langle \Delta M / \bar{M} \rangle$ with Ω_0 is of principal importance, not the actual value^{***}. Recall that in this paper we do not intend to compare $\langle \Delta M / \bar{M} \rangle$ directly to observations (§2.3), but rather we expect the next few moment ratios of the gravitational potential, which can be observed, to be strongly correlated with $\langle \Delta M / \bar{M} \rangle$ (see §2). Since 1-2 crossing times should effectively cover the reasonable range of relaxation timescales for potential fluctuations characterized by the lower order moments, the utility of $\langle \Delta M / \bar{M} \rangle$ for studying the dependence of cluster morphology is hardly affected by the uncertainty in the relaxation timescale. This behavior contrasts with that of δF (Richstone et al. 1992) and related measures (Lacey & Cole 1993) whose value is to be directly compared to the “frequency of substructure”.

Changing the value of σ_8 (equation 25) has virtually no effect on $\Delta M / \bar{M}$. For $\sigma_8 = 0.52, 1$ ($\Omega_0 = 1$) we find that $\Delta M / \bar{M}$ varies by $\lesssim 1\%$. This similarity occurs because the amplitude of $P(k)_{clus}$ arising from a higher σ_8 is mostly compensated for by a reduced cluster bias factor, b_{clus} . This insensitivity to $\sigma_8 = 0.5 - 1$ is also found in the mean $\log_{10} P_m/P_0$ distributions of BX.

Finally, we investigated the effect of using Ω_B appropriate for the gas fractions in clusters (White & Fabian 1995). In our models this only has the effect of slightly changing H_0 determined for a particular value of Ω_0 (see definition of Γ in §4). As a result, $\langle \Delta M / \bar{M} \rangle$ is essentially unaffected – we find results in excellent agreement with those obtained above with the BBN Ω_B . Of course, it would be better to test the effects of a greater baryon fraction by incorporating the gravitational dynamics of a dissipational component into the model.

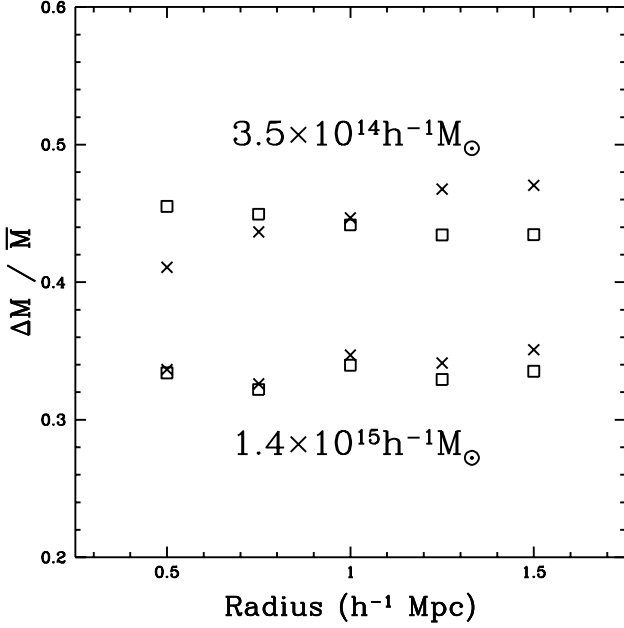


Figure 6. $\Delta M / \bar{M}$ versus radius for models with $\Omega_0 = 0.2$, $\lambda_0 = 0.8$ (boxes) and $\Omega_0 = 1$ (crosses).

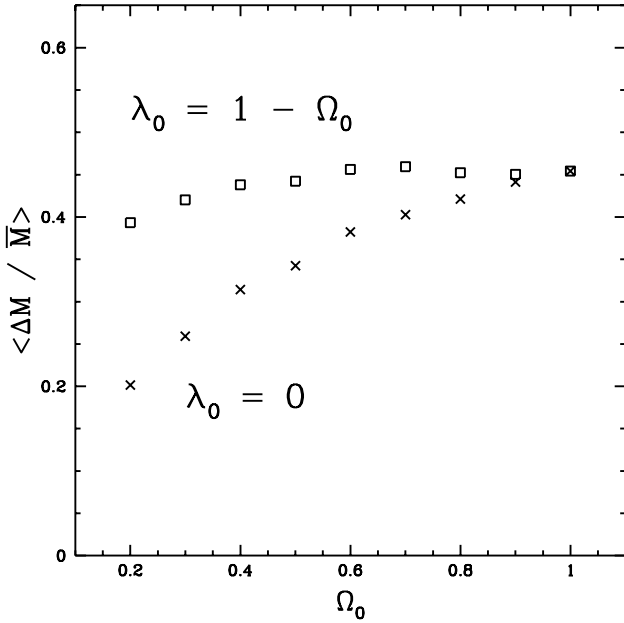


Figure 7. $\langle \Delta M / \bar{M} \rangle$ versus Ω_0 for $\Omega_0 + \lambda_0 = 1$ models (boxes) and $\lambda_0 = 0$ models (crosses). The relaxation timescale is $1t_{\text{cross}}$.

5.2.2 CDM: $\Omega_0 + \lambda_0 = 1$ at $z = 0$

We now turn our attention to the zero-curvature models, $\Omega_0 + \lambda_0 = 1$. In a low-density universe with zero-curvature only recently has the effect of a cosmological constant sig-

nificantly imprinted itself on the cosmic dynamics; i.e. the transition from $\Omega_0 \cong 1$ to $\Omega_0 < 1$ occurs considerably later and much more rapidly than in the $\lambda_0 = 0$ case. Hence, although the shells which collapsed at the present epoch turned around at times similar to those in $\lambda_0 = 0$ models, the previously collapsed shells turned around with times governed by a universe with $\Omega_0 \rightarrow 1$.

As a result, the density profiles of the zero-curvature models have essentially the same slope as the $\Omega_0 = 1$ models over radii $\sim (0.5 - 1)r_{200}$ (see §5.1). However, the profile of the zero-curvature models is flatter at smaller radii, $r \lesssim 0.2r_{200}$, indicating that the mean density within the central regions of the clusters is considerably smaller in zero-curvature models, consistent with the arguments given in §4 of Richstone et al. (1992). Because of this decrease in density, the half-mass radii are larger, the velocity dispersions smaller, and thus the crossing times (equation 19) are considerably larger in the low-density zero-curvature models than in their $\lambda_0 = 0$ counterparts: $t_{\text{cross}} = (0.20 - 0.23)/H_0$ over the full mass range for the $\Omega_0 = 0.2$ and $\lambda_0 = 0.8$ model, a factor of ~ 1.7 larger than the open $\Omega_0 = 0.2$ model. In fact, with respect to $\Omega_0 = 1$, t_{cross} is $\sim 40\%$ larger for the zero-curvature $\Omega_0 = 0.2$ model but $\sim 15\%$ smaller for the open $\Omega_0 = 0.2$ model. This considerably stronger and qualitatively different dependence of $\Delta M / \bar{M}$ on crossing time as a function of Ω_0 causes the low-density zero-curvature models to have qualitatively different behavior than their $\lambda_0 = 0$ counterparts.

We display in Figure 6 the radial profile of $\Delta M / \bar{M}$ for the $\Omega_0 = 0.2$, $\lambda_0 = 0.8$ model and the $\Omega_0 = 1$ model for a couple of representative masses. For $M \gtrsim 7 \times 10^{14} h^{-1} M_\odot$, the profile of the zero-curvature model is essentially flat but almost of the same magnitude as the $\Omega_0 = 1$ model. As expected, the differences between the models becomes most noticeable at larger radii because the accretion of the most recent shells is suppressed in the zero-curvature model; i.e. the recently collapsed shells approximately behave as in the $\Omega_0 = 0.2$, $\lambda_0 = 0$ case.

The $\Omega_0 = 0.2$ zero-curvature radial profile of $\Delta M / \bar{M}$ slightly decreases with radius for $M = 3.5 \times 10^{14} h^{-1} M_\odot$ and actually exceeds the $\Omega_0 = 1$ values for $r < 1 h^{-1}$ Mpc. This decreasing profile indicates that shells with turn-around radii $r_m \lesssim 2 h^{-1}$ Mpc dominate the contribution to $\Delta M / \bar{M}$ over the previous crossing time – since the crossing time is significantly larger than for $\Omega_0 = 1$, the zero-curvature model accretes shells at higher redshift which turned-around at smaller radii.

In Figure 7 we display $\langle \Delta M / \bar{M} \rangle$ versus Ω_0 for the zero-curvature models. In order to accentuate the dependence on Ω_0 we focus on the largest aperture considered, $r = 1.5 h^{-1}$ Mpc. We find that these models behave very nearly as $\Omega_0 = 1$ and depend only weakly on Ω_0 : $\langle \Delta M / \bar{M} \rangle \sim \Omega_0^{0.1}$. This behavior is qualitatively consistent with the linear growth of density fluctuations: the ratio of linear growth factors for the $\Omega_0 = 0.2$, $\lambda_0 = 0.8$ model to $\Omega_0 = 1$ is 0.70 compared to a ratio of 0.33 for the open $\Omega_0 = 0.2$ model to $\Omega_0 = 1$. That is, from linear growth we would expect the amount of accreted mass in clusters in the $\Omega_0 = 0.2$ zero-curvature model to be more similar to the $\Omega_0 = 1$ model than to the open $\Omega_0 = 0.2$ model (e.g. Peebles 1984). However, the N-body simulations of BX indicate that the means of the $\log_{10} P_m / P_0$ distributions of their zero-curvature mod-

*** This trend is quite insensitive to the slope of the power spectrum – see end of §5.2.4.

els, though intermediate with the $\Omega_0 = 0.35, 1$ cases they examined, nevertheless leaned more closely to the $\Omega_0 = 0.35$ open model for radii $(0.4 - 1.2)h^{-1}$ Mpc.

We emphasize that this weak Ω_0 -dependence arises from the increased crossing times for the low-density zero-curvature models. In Figure 5 we display $\Delta M_{ta}/\overline{M}_{ta}$ for the zero-curvature models with $t_{cross} = 0.14/H_0$ appropriate for the $\lambda_0 = 0$ models. In this case $\Delta M_{ta}/\overline{M}_{ta} \propto \Omega_0^{0.45}$ which is only slightly weaker than the Ω_0 -dependence for the $\lambda_0 = 0$ models. This $\sim \Omega_0^{0.45}$ dependence applies to $\langle \Delta M/\overline{M} \rangle$ if we fix $t_{cross} = 0.14/H_0$ for the zero-curvature models. (This behavior is also found for δF by Richstone et al. who also used a constant relaxation timescale for all models.)

Our procedure of setting the relaxation timescale equal to the crossing time is only an approximation. Because the crossing times in the zero-curvature models vary by almost a factor of 3 more than in the open models over $\Omega_0 = 0.2 - 1$, the accuracy associated with this procedure is considerably more important for studying the Ω_0 -dependence of $\Delta M/\overline{M}$ in the zero-curvature models.

In addition, other factors contribute to a computational uncertainty. Because the increase in crossing time is due primarily to the flatter density profile at small radii, the error due to the number of shells becomes more important. Also, issues like the smoothing length of the power spectrum become more important at radii $\lesssim 0.1r_{200}$. Hence, the detailed features in the profile of $\langle \Delta M/\overline{M} \rangle$ vs Ω_0 in Figure 7 (e.g. the $\Omega_0 \approx 0.7$ values exceeding $\Omega_0 = 1$) are probably due to the uncertainty in the relaxation timescale. Further study of the relaxation timescale for the zero-curvature models using three dimensional N-body simulations would certainly be of value here.

Nevertheless, it is clear that the low-density zero-curvature models do not mimic the corresponding open models and thus cluster morphologies do indeed distinguish between these two cases at $z = 0$ ***. We find that the difference between the models arises from the detailed virialized structure of the clusters (i.e. crossing times), which is consistent with the expectations of Lahav et al. (1991) that a cosmological constant, “could only have changed the density profile by its effect on the non-linear motion of shells.”

5.2.3 CDM: $z > 0$

Let us now consider the evolution of $\Delta M/\overline{M}$ with redshift in the context of the CDM model. For compactness we restrict our discussion to a relaxation timescale of $1t_{cross}$ and Ω_B equal to the BBN value. (The effect of different relaxation timescales is mentioned at the end of this section.) Since the cluster population becomes less massive with increasing z , we analyze $\Delta M/\overline{M}$ averaged over masses $[(0.7 - 3)/(1 + z)] \times 10^{15} h^{-1} M_{sun}$, where the $(1 + z)$ factor is intended to account for the reduction in mass according to

*** BX found that the means of the $\log_{10} P_m/P_0$ distributions of 39 simulated clusters for their $\Omega_0 = 0.35$ open and zero-curvature models, though systematically larger for the zero-curvature models as indicated by the non-overlapping error bars derived from bootstrap re-sampling, were formally consistent in terms of the Student’s-t test. It appears that a larger cluster sample is required to formally differentiate the means of the two models. This has been confirmed by Thomas et al. (1997).

the self-similar accretion law (Bertschinger 1985). We focus on a slightly higher mass range because a feasible observational sample either from lensing or X-rays will be biased towards more massive clusters. The qualitative results presented in this section remain if the lower limit on the mass average is halved.

In Figure 8 we display the radial profile of $\langle \Delta M/\overline{M} \rangle$ at $z = 0.4, 0.8$ for models with $\Omega_0 = 0.2, 1$ ($\lambda_0 = 0$) and $\Omega_0 = 0.2, \lambda_0 = 0.8$. Over redshifts $z \sim 0 - 0.4$ the behavior of $\langle \Delta M/\overline{M} \rangle$ with radius does not change appreciably. The shape of the open $\Omega_0 = 0.2$ profile remains constant over this interval, but the $\Omega_0 = 1$ profile shifts from being slightly increasing with radius (Figure 2) to slightly decreasing. As discussed in §5.2.2 for the zero-curvature models, the decreasing profile indicates that as z increases the clusters in the $\Omega_0 = 1$ models are growing faster in their inner regions; i.e. the accreted mass is dominated by shells with turn-around radii $\lesssim 2h^{-1}$ Mpc. This contrasts with the situation at $z = 0$ for the $\lambda_0 = 0$ models where the accretion of infalling shells contributes almost entirely to large radii, which is consistent with the behavior of the exact self-similar solution (Bertschinger 1985).

The shape of the fractional accreted mass profile of the zero-curvature $\Omega_0 = 0.2$ model is similar to that of the corresponding open model, but the normalization is similar to $\Omega_0 = 1$ as we found for the $z = 0$ case (with the same caveats regarding the crossing time effects discussed in §5.2.2). The profile of the zero-curvature $\Omega_0 = 0.2$ model does not decrease like the $\Omega_0 = 1$ model because the shells which affect most the outer radii are still determined by $\Omega_0 \approx 0.2$. That is, for the zero-curvature models the redshift indicating when the term involving the cosmological constant in the Friedmann equation dominates the matter term is given by, $(1 + z_{trans})^3 = \Omega_0^{-1} - 1$, after which linear growth is suppressed (e.g. §13 Peebles 1980). For $\Omega_0 = 0.2$, we have $z_{trans} = 0.6$.

Indeed, proceeding to higher redshift, $z = 0.8$, we see in Figure 8 that the profile of the zero-curvature $\Omega_0 = 0.2$ model now decreases with radius indicating that the matter term is beginning to dominate the Friedmann equation. The $\langle \Delta M/\overline{M} \rangle$ radial profile for $\Omega_0 = 1$ steepens while that for the open $\Omega_0 = 0.2$ model remains essentially flat. For redshifts $\gtrsim 1$ the profiles of the zero-curvature $\Omega_0 = 0.2$ model and $\Omega_0 = 1$ model have very similar shapes. Even the open model starts to steepen, though from the argument from linear theory we would not expect the transition to occur until approximately $z_{trans} = 3$. We emphasize, however, that the precise redshifts of these occurrences depend on the relaxation timescale. For longer relaxation timescales, these properties occur at lower redshifts and vice versa.

For the higher redshifts it is clear that the smaller aperture sizes optimize differences in Ω_0 ($\lambda_0 = 0$). In Figure 9 we show $\langle \Delta M/\overline{M} \rangle$ computed within a radius $0.5h^{-1}$ Mpc as a function of Ω_0 for $z = 0.4, 0.8$. Although the value of $\langle \Delta M/\overline{M} \rangle$ increases with increasing redshift indicating that the cluster morphologies are more disturbed, its sensitivity to Ω_0 decreases significantly with redshift: $\langle \Delta M/\overline{M} \rangle \approx 0.60\Omega_0^{0.29}$ for $z = 0.4$ and $\langle \Delta M/\overline{M} \rangle \approx 0.87\Omega_0^{0.23}$ for $z = 0.8$. (For comparison, for $r = 1.5h^{-1}$ Mpc we obtain $\langle \Delta M/\overline{M} \rangle \approx 0.67\Omega_0^{0.22}$ for $z = 0.4$ and $\langle \Delta M/\overline{M} \rangle \approx 0.75\Omega_0^{0.07}$ for $z = 0.8$.) The weakening trend with redshift is even observed as early

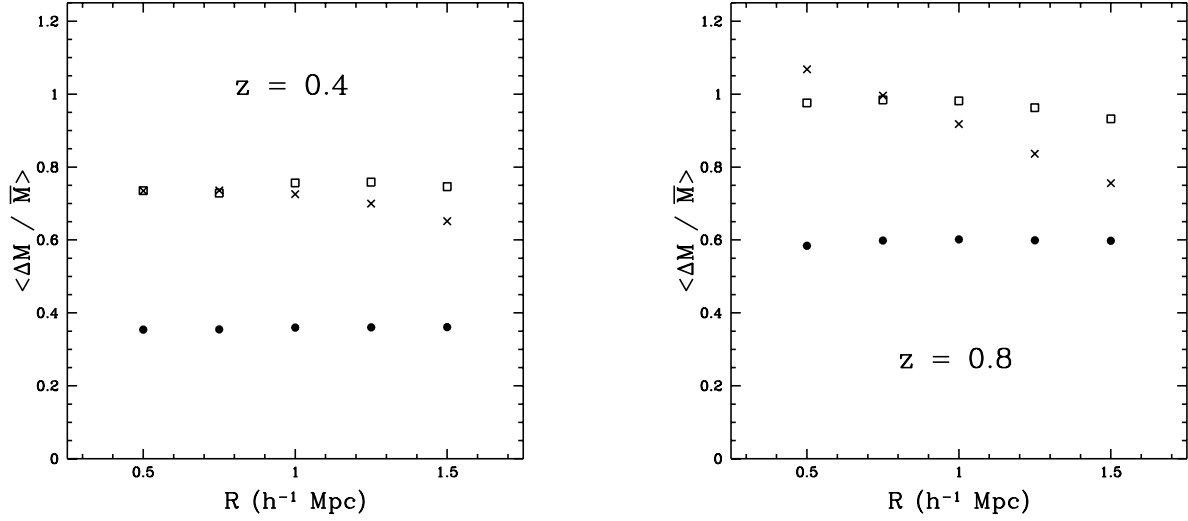


Figure 8. The radial profile of $\langle \Delta M / \bar{M} \rangle$ as a function of redshift for CDM models $\Omega_0 = 0.2$, $\lambda_0 = 0$ (filled circles), $\Omega_0 = 0.2$, $\lambda_0 = 0.8$ (boxes), and $\Omega_0 = 1$ (crosses). See text for details of the mass average.

as $z = 0.2$ where $\langle \Delta M / \bar{M} \rangle \approx 0.52\Omega_0^{0.37}$ in the $1h^{-1}$ Mpc aperture.

This decrease in the sensitivity to Ω_0 arises because of two effects. First, as z increases the dynamics of the universe approaches that of the Einstein-de Sitter case regardless of the present value of Ω_0 and λ_0 . Second, the relaxation timescale becomes an increasingly larger fraction of the age of the universe, and thus $\langle \Delta M / \bar{M} \rangle \rightarrow 2$ regardless of Ω_0 and λ_0 .

However, the decline in sensitivity to Ω_0 is more rapid for $\Delta M / \bar{M}$ than for $\Delta M_{ta} / \bar{M}_{ta}$. We find that the relationship $\Delta M_{ta} / \bar{M}_{ta} \sim \Omega_0^{1/2}$ holds from $z = 0$ until $z \approx 2$ at which point $\Delta M_{ta} / \bar{M}_{ta} \sim 2$ and the Ω_0 -dependence vanishes. Since $\Delta M_{ta} / \bar{M}_{ta}$ depends only on the turn-around times of shells and not the detailed virialized cluster structure, it scales more similarly to what is expected from linear theory: as remarked above, for the open $\Omega_0 = 0.2$ model the transition to the Einstein-de Sitter phase occurs approximately at $z_{trans} = 3$. However, this redshift is not reached because the crossing time is essentially the age of the universe at $z \approx 2$. Clearly, taking into account the detailed virialized structure of the clusters is important for higher redshifts.

5.2.4 Power law

Now we switch our focus to models having power-law power spectra. In Figure 10 we display $\Delta M / \bar{M}$ vs spectral index n at $z = 0$ for clusters of mass $7 \times 10^{14} h^{-1} M_\odot$; other masses have very similar profiles. For the moment we concentrate on models with $\Omega_0 = 1$ and have a relaxation time of $1t_{cross}$. The value of $\Delta M / \bar{M}$ for $n \approx -1.3$ agrees with the $\Omega_0 = 1$ CDM value as expected for clusters. The fractional accreted mass increases as n decreases and varies more over the range $n = 0, -2$ ($\Omega_0 = 1$) than it does as a function of Ω_0 for CDM models over the range $\Omega_0 = 0.2, 1$; $\Delta M / \bar{M} \approx 0.13(-n)^{5/2} + 0.15$.

This n -dependence may be understood in terms of the peaks formalism as follows. Peaks of a given height in $n = 0$

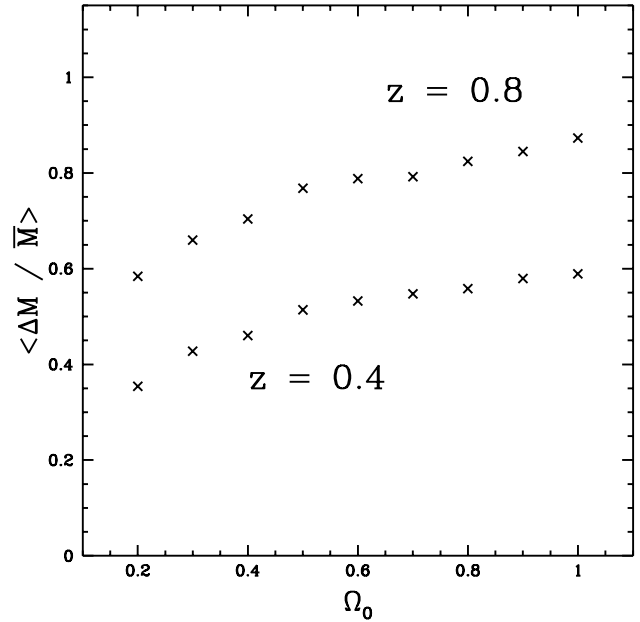


Figure 9. $\langle \Delta M / \bar{M} \rangle$ evaluated for $r = 0.5h^{-1}$ Mpc at $z = 0.4, 0.8$ for CDM models as a function of Ω_0 ($\lambda_0 = 0$). See text for details of the mass averaging.

models are much more isolated than peaks of similar height in $n = -2$ models; i.e. a cluster of mass $\sim 10^{15} h^{-1} M_\odot$ is an exceedingly rare high peak $\nu \sim 50$ in $n = 0$ models whereas such a cluster is a “normal” $\nu \sim 3$ peak for $n = -2$ models. Models with smaller n have more power on small scales and hence more possible mass to accrete at later times, which is to be regulated by the value of Ω_0 . Thus, regardless of the value of $\Omega_0 = 0.2 - 1$, the huge peak in the $n = 0$ model has a smaller value of $\Delta M / \bar{M}$ than the normal peak in $n = -2$ model.

However, real clusters are not $\nu \sim 50$ peaks. Here we

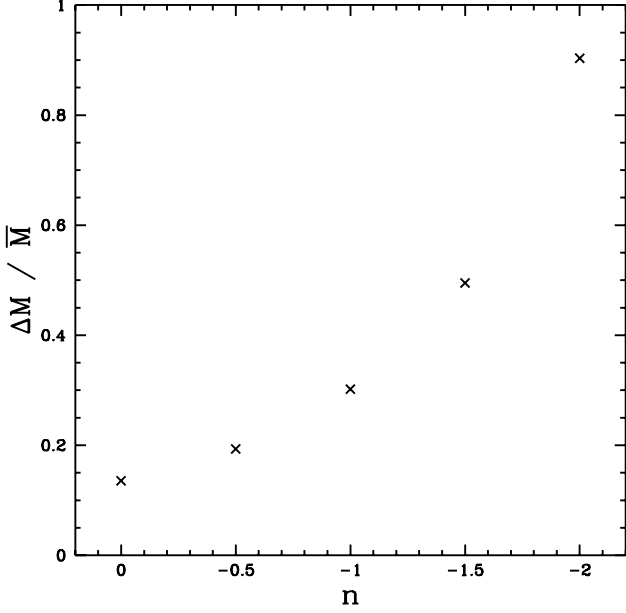


Figure 10. $\Delta M/\bar{M}$ for cluster of mass $7 \times 10^{14} h^{-1} M_{\odot}$ evaluated for $r = 1 h^{-1}$ Mpc at $z = 0$ for power-law models with $\Omega_0 = 1$ as a function of spectral index n .

experience the principal flaw in the peaks formalism in that merging is not taken into account (although see Bond & Myers 1996), which particularly affects models with $n \geq -1$ because in this case the collapse dynamics of a peak is not dominated by its initial density distribution (Bernardeau 1994). We have argued (see §2) that the effects of merging should not affect the mean of $\Delta M/\bar{M}$ when averaged over a cluster sample which is most relevant for studying Ω_0 . Rather, the fluctuations induced in $\Delta M/\bar{M}$ by mergers necessarily affects the variance.

To understand this qualitatively let us envision clusters formed in $n = 0, -2$ models considering the effects of mergers. In the $n = 0$ model, since there is little mass on smaller scales for a cluster of reasonable peak height to accrete, $\Delta M/\bar{M}$ will tend to be small for many clusters. However, when a cluster merges with another of comparable size (it will be similar in size since there is little small-scale mass) $\Delta M/\bar{M}$ will be comparatively large. In comparison, clusters in the $n = -2$ model have significant small-scale mass to accrete so $\Delta M/\bar{M}$ will not vary as much from cluster to cluster as in the $n = 0$ model; i.e. when averaged over a sample of $n = 0$ clusters, $\Delta M/\bar{M}$ will have a broader distribution than in the $n = -2$ model.

The three dimensional N-body simulations of BX support this qualitative picture: the distributions of $\log_{10} P_m/P_0$ for the $n = 0$ model indeed have significantly larger variances than for $n = -2$. (But the means of the distributions are largely the same.) Hence, for studying the effect of the slope of the power spectrum on the relationship between $\Delta M/\bar{M}$ and Ω_0 merging must be properly taken into account. Since our spherical model does not account for the effects of mergers, it is imperative to keep the shape of the power spectrum approximately fixed when comparing models with different Ω_0 as we have done in the previous sec-

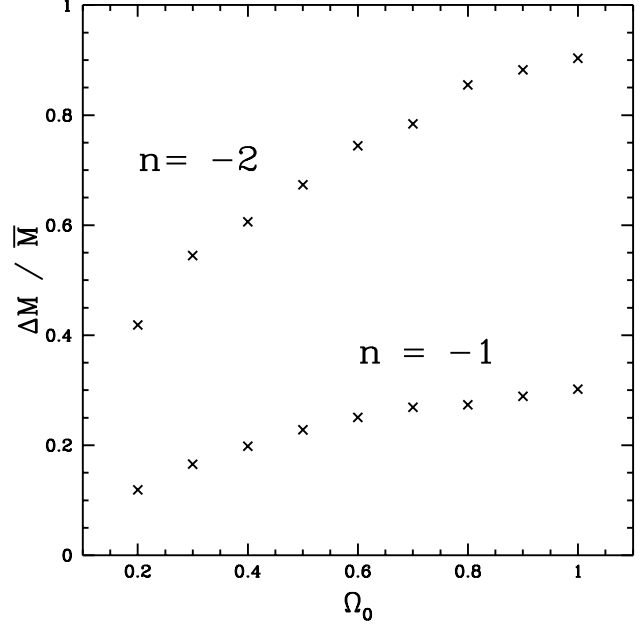


Figure 11. $\Delta M/\bar{M}$ vs Ω_0 for power-law models with $n = -1, -2$ for clusters of mass $7 \times 10^{14} h^{-1} M_{\odot}$ evaluated for $r = 1 h^{-1}$ Mpc at $z = 0$.

tions. It is also imperative to insure that the effective n on cluster scales is less than -1 so that the collapse dynamics is determined mostly by the initial peak density distribution (Bernardeau 1994).

Although it is important when comparing $\Delta M/\bar{M}$ for models with different Ω_0 to insure that n is approximately fixed, the value of n is not important. In Figure 11 we show $\Delta M/\bar{M}$ as a function of Ω_0 for power-law models with $n = -1, -2$. Although the values of the $n = -2$ models are approximately double those of the $n = -1$ models, the dependence on Ω_0 is similar in each: $\Delta M/\bar{M} \approx 0.31 \Omega_0^{0.51}$ for $n = -1$ and $\Delta M/\bar{M} \approx 0.93 \Omega_0^{0.46}$ for $n = -2$.

6 DISCUSSION AND CONCLUSIONS

We have constructed a simple, intuitive model to study the dependence of substructure in clusters on Ω_0 , λ_0 , and z . We characterize the importance of substructure and non-ellipsoidal features in the mass of a cluster, or equivalently the dynamical state, in terms of, $\Delta M/\bar{M}$, the fractional amount of mass accreted over the previous relaxation time within a radius r , where ΔM is the mass increase and \bar{M} is the average mass within r over the relaxation time. This fractional accreted mass is the monopole term in the multipole expansion of the fractional increase in the gravitational potential due to matter interior to r . Since, by hypothesis, $\Delta M/\bar{M}$ determines the importance of substructure and non-ellipsoidal features, it must strongly correlate with the next few multipole terms which are approximately the ratios, $\Phi_l^{int}/\Phi_0^{int}$.

These multipole ratios, or rather their projected counterparts, $P_m/P_0 \equiv \langle (\Psi_m^{int})^2 \rangle / \langle (\Psi_0^{int})^2 \rangle$, are directly observable and share the same type of correlation with $\Delta M/\bar{M}$

(see §2.2). With N-body simulations the correlations between $\Delta M/\overline{M}$ and P_m/P_0 can be explicitly quantified and thus allow a measurement of Ω_0 to be obtained directly from cluster observations with gravitational lensing and X-rays. In this paper we have examined the differences of $\Delta M/\overline{M}$ in models with different Ω_0 (and $P(k)$) which are related to the differences in P_m/P_0 without requiring knowledge of the actual correlation. (The reasonable agreement found for the mean shift between $\Omega_0 = 1$ and $\Omega_0 = 0.35$ for the P_m/P_0 of the N-body clusters in BX and $\Delta M/\overline{M}$ provides quantitative justification for this procedure – see §5.2.1.) That is, we predict how the low order P_m/P_0 should behave with Ω_0 , λ_0 , and z . In this way we can acquire intuition of how clusters evolve dynamically in different cosmologies, and, as we discuss below, we can identify the best ways to constrain Ω_0 , λ_0 with much greater ease than via computationally expensive three dimensional N-body simulations. We compute $\Delta M/\overline{M}$ using the spherical accretion model in the adiabatic approximation of Ryden & Gunn (1987).

Our model extends and improves upon previous studies in several respects. First, we compute complete one-dimensional mass distributions of clusters using the spherical accretion model, where the initial density profiles of the clusters are given by the peaks formalism (BBKS). The relaxation time, taken to be a multiple of the crossing time, is computed individually for each cluster. In contrast, previous studies (Richstone et al. 1992; Kauffmann & White 1993; Lacey & Cole 1993) did not compute mass distributions of individual clusters and assumed a constant relaxation timescale for all clusters. Moreover, Richstone et al. assumed clusters arise from homogeneous density fluctuations on one particular mass scale.

The principal difference, however, between our work and the previous studies mentioned above lies in how they relate to observations. The previous studies predict the fraction of clusters that are expected to show evidence of substructure. In terms of observations this is generally referred to as the “frequency of substructure” and interpreted as the fraction of observed clusters that exhibit multiple density peaks. Because these previous theoretical studies do not indicate the type of substructure or morphological features to be seen in clusters, it is unclear how to compare their predictions with observations; i.e. what sizes of multiple density peaks are required before a cluster is to be considered unformed? This ambiguity is resolved in our model because $\Delta M/\overline{M}$ is expected to correlate strongly with $\Phi_l^{int}/\Phi_0^{int}$ for small l and with $\Psi_m^{int}/\Psi_0^{int}$ for small m . These multipole ratios quantify the cluster morphology explicitly.

Because the previous studies do not specify the type of substructure, the relaxation timescale (or rather the survival time of substructure) is very uncertain – with some studies indicating uncertainty up to $\sim 1 - 10$ crossing times (Nakamura et al. 1995). Since the predicted “frequency of substructure” is highly sensitive to the substructure survival time, the predictions made by the previous studies are too uncertain to be useful (Kauffmann & White 1993; Lacey & Cole 1993). In our model, the relevant relaxation timescale is realistically confined to $\sim 1 - 2$ crossing times since $\Delta M/\overline{M}$ is concerned only with the low order moments in the cluster potential (i.e. large potential fluctuations containing $\gtrsim 20\%$ of the total cluster mass). Moreover, since it is only the expected correlation of $\Delta M/\overline{M}$ with the low order moments

that we require, and not the actual value, the uncertainty associated with $\sim 1 - 2$ crossing times is unimportant for our present study of Ω_0 (§5.2.1).

The results of our study suggest the following procedure to optimize constraints on Ω_0 and λ_0 from analysis of cluster morphologies quantified in terms of P_m/P_0 . The present epoch exhibits the strongest dependence of cluster morphologies on Ω_0 with $\langle \Delta M/\overline{M} \rangle \sim \Omega_0^{1/2}$ – the higher mass clusters $M \gtrsim 7 \times 10^{14} h^{-1} M_\odot$ are slightly preferred for this purpose. At $z = 0$, $\langle \Delta M/\overline{M} \rangle$ depends only weakly on radius. However, P_m/P_0 declines with radius because the higher order moments give way to the monopole term as the radius is increased. Hence, any $r \lesssim 1 h^{-1}$ would seem best in this light. (Although not too small to invalidate the connection between the 2-D and 3-D monopoles – §2.2.)

Although the dependence of $\langle \Delta M/\overline{M} \rangle$ weakens with increasing redshift, analyzing high-redshift data separately and combining with $z = 0$ data significantly improves the ability to constrain models. First, simply obtaining independent cluster samples at medium ($z \sim 0.4$) and high ($z \sim 0.8$) redshifts and combining with $z = 0$ data increases the dependence on Ω_0 from $\sim \Omega_0^{1/2}$ at $z = 0$ to $\sim \Omega_0^{1/2} \times \Omega_0^{0.29} \times \Omega_0^{0.23} \sim \Omega_0$. Second, the evolution of $\langle \Delta M/\overline{M} \rangle$ with z depends on Ω_0 as well: the ratio of $\langle \Delta M/\overline{M} \rangle$ for $z = 0.8$ and $z = 0$ models goes approximately as $\Omega_0^{-1/4}$ indicating that the morphologies of clusters in a low-density universe undergo more rapid evolution than if $\Omega_0 = 1$ thereby providing an additional constraint. Finally, the radial dependence of $\langle \Delta M/\overline{M} \rangle$ is very different for $\Omega_0 = 0.2, 1$ models over radii $(0.5 - 1.5) h^{-1}$ Mpc, and we would expect that P_m/P_0 would decrease with radius considerably more rapidly for $z \gtrsim 0.5$ if $\Omega_0 = 1$ than if $\Omega_0 = 0.2$ with or without a cosmological constant.

Because the dependence of $\Delta M/\overline{M}$ on Ω_0 weakens with increasing redshift, X-ray observations of clusters have a clear advantage over gravitational lensing observations since the latter are essentially restricted to $z \gtrsim 0.15$. Moreover, the P_m/P_0 computed on the X-ray surface brightness distributions of clusters have a larger dynamic range than those computed on the projected mass distributions (§4 of Tsai & Buote 1996), which probably translates to a greater sensitivity for probing Ω_0 (see end of §2.2). For $z \gtrsim 0.2$, both X-ray and lensing observations are well suited for probing the evolution of cluster morphologies with redshift. However, the theoretical comparison for lensing data only requires dissipationless simulations which is a definite advantage over the more computationally expensive dissipational simulations required for the comparison to X-ray data.

Although we believe at present that further refinements to our model are not justified given the uncertainty in the relaxation time and the qualitative nature of the relationship between $\Delta M/\overline{M}$ and the low order multipole ratios, there are areas which could use some attention. A study quantifying the relationship between $\Delta M/\overline{M}$, $\langle (\Phi_l^{int})^2 \rangle^{1/2} / \langle (\Phi_0^{int})^2 \rangle^{1/2}$, and P_m/P_0 using N-body simulations would help clarify predictions of this model (i.e. determine c_m and d_m – see §2.2), and will enable a direct comparison to observations of cluster surface density maps obtained from gravitational lensing and X-ray data. If such a study can also significantly limit the range of relaxation times for low order potential fluctuations, then investigation

of the secondary effects such as non-sphericity and angular momentum may be warranted.

To illustrate the potential for such studies, let us compare $\Delta M/\overline{M}$ to the P_m/P_0 computed in §4 of Tsai & Buote (1996) for the dark matter (i.e. ρ as opposed to ρ^2) of clusters formed in a $\Omega_0 = 1$ CDM simulation. The even P_m/P_0 are nearly proportional to each other such that $P_2/P_0 \approx 100P_4/P_0$, and the mean value of P_2/P_0 is $\sim 10^{-4}$. If we assume the same scaling applies to the monopole, i.e. $(\Delta M/\overline{M})^2 \approx 100P_2/P_0$, then we estimate $\Delta M/\overline{M} \approx 0.10$. This value is in qualitative agreement with the value of ≈ 0.4 we determined in §5.2.1. Since the magnitude of $\Delta M/\overline{M}$ scales approximately linearly with relaxation time, this suggests that the appropriate relaxation timescale for the low order multipoles is $< 1t_{cross} = 0.14/H_0$.

Hence, cluster morphologies would appear to be an attractive means to probe Ω_0 and λ_0 . Theoretically, cluster morphologies are related to Ω_0 and λ_0 in a conceptually straightforward way, are sensitive to λ_0 at $z = 0$, and are very insensitive to Ω_B (§5.2.1) and the cluster bias factor unlike some other indicators for Ω_0 (Dekel et al. 1996). Observationally, cluster morphologies are easy to quantify in terms of P_m/P_0 (Buote & Tsai 1996). The challenge lies in acquiring lensing and X-ray data of large samples ($\gtrsim 50$) of clusters at various redshifts for comparison to large, high-resolution N-body simulations of lensing maps and hydrodynamic simulations of X-ray images.

Alternatively, if N-body simulations confirm that the correlations between $\Delta M/\overline{M}$ and the low order P_m/P_0 are tight and mostly independent of Ω_0 , then the N-body simulations will only be needed to initially calibrate this correlation. In this case subsequent comparison of $\Delta M/\overline{M}$ to observations can be achieved rapidly using the spherical accretion model and allow Ω_0 and λ_0 to be determined with considerably less computational expenditure than required for the standard method.

ACKNOWLEDGMENTS

We thank P. Natarajan and S. Sigurdsson for comments on the manuscript. We also thank the anonymous referee for suggesting that we emphasize the direct application of this model to observations (§2.2).

APPENDIX A: SPHERICAL MODEL FOR CASE $\Omega_0 + \lambda_0 = 1$

Here we give the formulae for the radius and time at maximum expansion of spherical shells evolving in a universe where $\Omega_0 + \lambda_0 = 1$ (see §3.2). Related expressions may be found in Richstone et al. (1992) for the case of homogeneous density perturbations, and in Eke et al. (1996), who adopt the equations of Peebles (1984) which assume a particular initial condition, $a = r$ at $z \rightarrow \infty$, where a is the expansion factor and r is the proper radius of the mass shell. We give expressions explicitly defined for an arbitrary initial epoch.

We begin with the energy integral for a spherical perturbation in a universe with non-zero cosmological constant $\Lambda \equiv 3H_i^2 \lambda_i$,

$$E = \frac{1}{2} \left(\frac{dr}{dt} \right)^2 - \frac{GM(< r)}{r} - \frac{1}{6} \Lambda r^2, \quad (A1)$$

which is conserved before shell-crossing. The mass enclosed within proper radius r is,

$$M(< r) = \frac{4\pi}{3} \rho_b(t_i) (1 + \overline{\delta}_i) r_i^3, \quad (A2)$$

where $\rho_b(t_i)$ is the density of the background universe and r_i the proper radius at the initial time t_i which has expanded to radius r at a time $t \leq t_m$. The energy evaluated at t_i is,

$$E_i = -K_i \Omega_i \overline{\delta}_i, \quad (A3)$$

where $K_i = H_i^2 r_i^2 / 2$ is the initial kinetic energy and we have neglected peculiar velocities and set $\lambda_i = 1 - \Omega_i$. At maximum expansion the energy is all potential,

$$E_m = \frac{r_i}{r_m} (-K_i \Omega_i [1 + \overline{\delta}_i]) + \left(\frac{r_m}{r_i} \right)^2 (-K_i [1 - \Omega_i]), \quad (A4)$$

where r_m is the proper radius at maximum expansion. Since the energy is conserved we may set $E_m = E_i$ and obtain an equation for r_m/r_i ,

$$\frac{\Omega_i^{-1} - 1}{1 + \overline{\delta}_i} \left(\frac{r_m}{r_i} \right)^3 - \frac{\overline{\delta}_i}{1 + \overline{\delta}_i} \left(\frac{r_m}{r_i} \right) + 1 = 0, \quad (A5)$$

which has the standard cubic solution,

$$\frac{r_m}{r_i} = \frac{2}{\sqrt{3}} \left(\frac{\overline{\delta}_i}{\Omega_i^{-1} - 1} \right)^{1/2} \cos \left(\frac{\Theta}{3} + \frac{\pi}{3} \right), \quad (A6)$$

where,

$$\cos \Theta = \frac{3^{3/2}}{2} \frac{1 + \overline{\delta}_i}{\Omega_i^{-1} - 1} \left(\frac{\Omega_i^{-1} - 1}{\overline{\delta}_i} \right)^{3/2}, \quad (A7)$$

for $0 \leq \Theta \leq \pi/2$. Finally, by setting the energy before maximum expansion equal to the initial energy we obtain an equation for the time as a function of r . The time corresponding to maximum expansion is thus,

$$t_m = t_i + H_i^{-1} \Omega_i^{-1/2} (1 + \overline{\delta}_i)^{-1/2} \times \int_1^{r_m/r_i} dR \sqrt{R} \left(\frac{\Omega_i^{-1} - 1}{1 + \overline{\delta}_i} R^3 - \frac{\overline{\delta}_i}{1 + \overline{\delta}_i} R + 1 \right)^{-1/2} \quad (A8)$$

REFERENCES

- Anninos P., Norman M. L., 1996, ApJ, 459, 12
- Antonuccio-Delogu V., Colafrancesco S., 1994, ApJ, 427, 72
- Bardeen J. M., Bond J. R., Efstathiou G., 1987, ApJ, 321, 28
- Bardeen J. M., Bond J. R., Kaiser N., Szalay A. S., 1986, ApJ, 304, 15
- Bartelmann M., Ehlers J., Schneider P., 1993, A&A, 280, 351
- Bernardeau F., 1994, ApJ, 427, 51
- Bertschinger E., 1985, ApJS, 58, 39
- Binney J., Tremaine S., 1987, Galactic Dynamics. Princeton Univ. Press, Princeton
- Blumenthal G. R., Faber S. M., Flores R., Primack J. R., 1986, ApJ, 301, 27
- Bond J. R., Myers S. T. 1996, ApJS, 103, 1
- Bond J. R., Cole S., Efstathiou G., Kaiser N., 1991, ApJ, 379, 440
- Buote D. A., 1997, in preparation
- Buote D. A., Canizares C. R., 1994, ApJ, 427, 86
- Buote D. A., Canizares C. R., 1996, ApJ, 457, 177
- Buote D. A., Tsai J. C., 1995, ApJ, 452, 522

- Buote D. A., Tsai J. C., 1996, *ApJ*, 458, 27
- Buote D. A., Xu G., 1997, *MNRAS*, 284, 439 (BX)
- Carlberg R. G., Yee H. K. C., Ellingson E., 1997, *ApJ*, 478, 462
- Carroll S. M., Press W. H., Turner E. L., 1992, *ARA&A*, 30, 499
- Cole S., Lacey C., 1996, *MNRAS*, 281, 716
- Copi C., Schramm D. N., Turner M. S., 1995, *Science*, 267, 192
- Croft R. A., Efstathiou G., 1994, *MNRAS*, 267, 390
- Dekel A., Burstein D., White S. D. M., 1996, in Turok N., ed., *Critical Dialogues in Cosmology* (Princeton 250th Anniversary), World Scientific, in press
- Del Popolo A., Gambera M., 1997, *A&A*, submitted
- Efstathiou G., Dalton G. B., Sutherland W. J., Maddox S. J., 1993, *MNRAS*, 257, 125
- Eke V. R., Cole S., Frenk C. S., 1996, *MNRAS*, 282, 263
- Fabian A. C., 1994, *ARA&A*, 32, 277
- Fillmore J. A., Goldreich P., 1984, *ApJ*, 281, 1
- Frenk C. S., White S. D. M., Efstathiou G., Davis M., 1990, *ApJ*, 351, 10
- Fukugita M., Hogan J. C., Peebles P. J. E., 1993, *Nature*, 336, 309
- Gunn J. E., 1977, *ApJ*, 218, 592
- Hoffman Y., 1988, *ApJ*, 328, 489
- Jing Y. P., Mo H. J., Börner G., Fang L. Z., 1995, *MNRAS*, 276, 417
- Kauffmann G., White S. D. M., 1993, *MNRAS*, 261, 921
- Lacey C., Cole S., 1993, *MNRAS*, 262, 627
- Lahav O., Lilje P. B., Primack J. R., Rees M. J., 1991, *ApJ*, 251, 128
- Lilje P. B., Lahav O., 1991, *ApJ*, 374, 29
- Lynden-Bell D., 1967, *MNRAS*, 136, 101
- Mo H. J., Jing Y. P., White S. D. M., 1997, *MNRAS*, 282, 1086
- Nakamura F. E., Hattori M., Mineshige S., 1995, *A&A*, 302, 649
- Natarajan P., Hjorth J., van Kampen E., 1997, *MNRAS*, 286, 329
- Navarro J. F., Frenk C. S., White S. D. M., 1995, *MNRAS*, 275, 720
- Navarro J. F., Frenk C. S., White S. D. M., 1997, *MNRAS*, submitted (astro-ph/9611107)
- Ostriker J. P., 1993, *ARA&A*, 31, 689
- Padmanabhan T., 1993, *Structure Formation in the Universe*. Cambridge Univ. Press, Cambridge
- Peacock J. A., 1997, *ApJ*, 284, 885
- Peacock J. A., Dodds S. J., 1994, *ApJ*, 267, 1020
- Peebles P. J. E., 1980, *The Large-Scale Structure of the Universe*. Princeton Univ. Press, Princeton
- Peebles P. J. E., 1984, *ApJ*, 284, 439
- Press W. H., Schechter P., 1974, *ApJ*, 187, 452
- Richstone D. O., Loeb A., Turner E. L., 1992, *ApJ*, 393, 477
- Ryden B. S., 1988, *ApJ*, 333, 78
- Ryden B. S., Gunn J. E., 1987, *ApJ*, 318, 15
- Sahni V., Coles P., 1995, *Physics Reports*, 262, 1
- Sigurdsson S., Hernquist L., Quinlan G. D., 1995, *ApJ*, 446, 75
- Sugiyama N., 1995, *ApJS*, 100, 281
- Thomas P. A., et al., 1997, *MNRAS*, submitted (astro-ph/9707018)
- Thoul A. A., Weinberg D. H., 1995, *ApJ*, 442, 480
- Tormen G., Bouchet F. R., White S. D. M., 1997, *MNRAS*, 286, 865
- Tsai J. C., Buote D. A., 1996, *MNRAS*, 282, 77
- Viana P. T. P., Liddle A. R., 1996, *MNRAS*, 281, 323
- White D. A., Fabian A. C., 1995, *MNRAS*, 273, 72
- White S. D. M., Efstathiou G., Frenk C. S., 1993, *MNRAS*, 262, 1023
- White S. D. M., Rees M. J., 1978, *MNRAS*, 183, 341
- Zaroubi S., Naim A., Hoffman Y., 1996, *ApJ*, 457, 50